ADVANCING EARTH AND SPACE SCIENCE

JGR Planets

RESEARCH ARTICLE
10.1029/2019JE006258

Dynamics of Lithospheric Overturns and Implications for Venus's Surface

S. Uppalapati[1], T. Rolf[1], F. Crameri[1], and S. C. Werner[1]

[1]Centre for Earth Evolution and Dynamics (CEED), Department for Geosciences, University of Oslo, Oslo, Norway

Key Points:
- Episodic-lid models predict thinner crust and older surface than stagnant-lid models
- Both stagnant and episodic regime predict substantial lateral variation in surface age
- Our episodic-lid model captures Venus's age and crustal characteristics better

Supporting Information:
- Supporting Information S1

Correspondence to:
S. Uppalapati and S. C. Werner,
sruthi.uppalapati@geo.uio.no;
stephanie.werner@geo.uio.no

Citation:
Uppalapati, S., Rolf, T., Crameri, F., & Werner, S. C. (2020). Dynamics of lithospheric overturns and implications for venus's surface. *Journal of Geophysical Research: Planets*, *125*, e2019JE006258. https://doi.org/10.1029/2019JE006258

Received 30 OCT 2019
Accepted 7 OCT 2020

Abstract Venus is currently characterized by stagnant-lid mantle convection, but could have previously experienced episodes of global resurfacing due to lithospheric overturn. Using numerical models of Venus's interior, we attempt to explain Venus's surface characteristics in the context of interior evolution and to understand how Venus's tectonic history has diverged from Earth's. For both the stagnant- and the episodic-lid regime, we explore the role of reference mantle viscosity; for the latter regime, we also explore the role of the lithospheric yield stress. Our stagnant-lid models predict thicker crust and younger surface than typically inferred from cratering statistics. When considering resurfacing episodes, the yield stress influences the frequency of overturns, which limits crustal thickness to better agree with previous independent estimates. Surface age is variable and depends on overturn frequency and resurfacing rate between overturns but reaches larger values just before an upcoming overturn event compared to values in the stagnant-lid cases. Both regimes predict substantial lateral variations in surface age, instead of an end-member uniform surface age indicating the cessation time of the last overturn, because ongoing volcanic resurfacing is spatially heterogeneous and dominates over tectonic resurfacing. Reviewing the crater-based surface age variations suggests that the model-predicted age spreads in the episodic scenario could be consistent with Venus's cratering record. Moreover, we find that a small fraction of crust can resist recycling during overturns. These outcomes indicate that overturn events may allow for surface age variations that reproduce Venus's surface better than stagnant-lid models.

Plain Language Summary In contrast to Earth, Venus currently does not feature plate tectonics inhibiting effective crustal recycling into the planetary interior. Yet, its surface features only few and almost randomly distributed craters, which suggests a globally young and more homogeneous surface age than on other planetary surfaces. To date, it remains unclear whether these surface characteristics are generated in an equilibrium style of resurfacing due to volcanism or whether large-scale tectonic overturns are required to explain the observations. Here, we use numerical models of Venus's interior evolution to predict the planet's surface characteristic like crustal thickness and surface age in two geodynamic regimes, either with or without tectonic overturns. With overturns, predicted mean crustal thickness and mean surface age are closer to other independent estimates. Both regimes predict substantial lateral variations of surface age (which is thus nonuniform), because even if global resurfacing happens at a time, ongoing and spatially heterogeneous volcanism modifies the age distribution subsequently. However, inspection of independent Venus crater-based surface ages and geological mapping reveals that our predicted variations using an episodic scenario could be consistent with the planet's cratering record. Within our modeling framework, the episodic regime seems thus more promising to explain Venus's surface age characteristics.

1. Introduction

Across the solar system, planetary surfaces and specifically their volcano-tectonic structures offer windows into the dynamic evolution of planetary interiors. Volcanism and tectonism rejuvenate the planetary surface depending on the rate and style of magmatic and tectonic processes. While the present Earth's surface is, at the large scale, dominated by ocean-plate tectonics (Crameri et al., 2019), other bodies' surfaces are either dominated by extensive volcanism (e.g., Io) or show very little to no sign of recent activity. The latter is the case for the classical stagnant-lid bodies, Mars, Mercury, and the Moon, which feature a strong immobile lithosphere; the global-scale convection is or was (if convection ceased at some point) restricted to the mantle region below this so-called stagnant lid. Venus, however, appears as a special case and may be an example of a body with a lithosphere somewhere in between the limits of the above end-members.

Venus's present surface does not feature any indication for ongoing plate tectonics as on Earth. The rate (if any) at which the planet recycles its crust is not clear and could, for example, invoke entrainment of lower crust by convective mantle downwelling (Lenardic et al., 1993). However, the surface shows signs of a variety of different styles of surface deformation, even subduction-like structures (Davaille et al., 2017; Sandwell & Schubert, 1992). Detailed mapping of Magellan radar observations and Venera images revealed large extensional ridge belts and quasi-circular features matching terrestrial subduction structures, which gave rise to the idea of recent activity and large-scale tectonic resurfacing on Venus (Frank & Head, 1990; Hansen & Phillips, 1995). Venus's essentially random distribution of impact craters (Schaber et al., 1992) has consequences for interpreting the crater record with regards to surface age. One end-member interpretation is that the whole planet was resurfaced by one catastrophic event (Ivanov & Head, 2013; Lenardic et al., 1993; Strom et al., 1994; Turcotte et al., 1999), which would imply a close-to-uniform surface age. Compared to the very old surfaces of the Moon, Mars, or Mercury, the low crater density suggests a surface age of $\sim 750^{+350}_{-400}$ Myr (Hauck et al., 1998; McKinnon et al., 1997; Nimmo & McKenzie, 1998; Strom et al., 1994), but some recent studies have even proposed ages as low as 150–250 Myr (Herrick & Rumpf, 2011; Le Feuvre & Wieczorek, 2011). Clearly, such a rapid, global resurfacing event is an end-member and using statistical arguments it could well be that a number of several, smaller-scale events determined Venus's surface distribution (see e.g., Hauck et al., 1998). In the extreme case, there could be many events that affect only a small and spatially random surface fraction, so that resurfacing is not characterized by distinct episodes any longer, but more in equilibrium. However, the observed size distribution of the mapped volcanic units excludes the pure equilibrium end-member, because the largest volcanic plain units are too large (Romeo & Turcotte, 2010).

The frequency and lateral extent of global resurfacing events during Venus's evolution can hardly be constrained from present-day observations since no rocks older than the latest event would persist at the surface. Therefore, the idea of less catastrophic resurfacing provides a more straightforward explanation for how Venus's complex geological surface structure with many different geological units of different age could have been generated (Ivanov & Head, 2011; Kreslavsky et al., 2015).

These and other issues have motivated researchers to find alternatives to both resurfacing end-members, involving either catastrophic global overturns or equilibrium volcanic resurfacing. The latter end-member, with resurfacing happening more continuously but at a much reduced rate, has been suggested to match the constraints from crater statistics similarly well as the catastrophic overturn scenario (Bjonnes et al., 2012). Yet, the capacity of equilibrium resurfacing to match observations remains debated (Kreslavsky et al., 2015; O'Rourke et al., 2014; Romeo, 2013; Romeo & Turcotte, 2010). After all, it is difficult to infer Venus's governing surface tectonic regime and its history in the context of the existing sparse observations.

Numerical models have thus widely been applied to investigate Venus's interior evolution and the dynamic causes of resurfacing. King (2018) computed 3D spherical models of thermal convection and concluded that an episodic overturn regime conflicts with the observed small offset between Venus's center of mass and center of figure (Bindschadler et al., 1992). However, this depends on timing: the more time has passed since the latest overturn, the weaker will be relics of it in the Venusian mantle. Rolf et al. (2018) showed that many of the overturn effects are limited to a couple of 100 Myr after overturn cessation, with the region above the core-mantle boundary (CMB) being affected the longest, as most recycled surface material eventually ends up there. This crucially depends on the composition and density structure of the mantle and the recycled surface material as well as the associated mineral phases (e.g., Papuc & Davies, 2012). Such complexities were investigated by Armann and Tackley (2012) with the conclusion that an episodic style of mantle convection with pronounced resurfacing events helps limiting the rate of magmatism and crustal growth. The same conclusion was reached by Rolf et al. (2018) using 3D geometry. In their stagnant-lid models, predicted crustal thickness exceeded other independent estimates significantly (Anderson & Smrekar, 2006; James et al., 2013; Jiménez-Díaz et al., 2015; Wei et al., 2014), while the episodic regime was more successful at approaching these estimates. Rolf et al. (2018) did not investigate the center of mass-center of figure offset (King, 2018) but, for the rest of the long-wavelength gravity spectrum (spherical harmonic degrees 2–16), the match to the observations was as good as or even better in the episodic than in the stagnant-lid models. The authors also concluded that episodic overturns facilitate the generation of a surface age comparable to the classic estimates of, for instance, McKinnon et al. (1997). The resurfacing events modeled by Rolf et al. (2018) tended to mobilize the surface globally, but the authors did not closely investigate whether parts of the surface resist recycling during these events. Such a tendency has recently been modeled by Weller and Kiefer (2020). In any case, what is observed on the present surface of Venus would be strongly shaped by an overturn event. The interpretation of the surface record is dependent on the timing of the overturn events, in particular the latest, as well as on how much of the internal magmatic activity manifests itself in the form of volcanism and crustal growth on the surface after the event has ceased.

Up to now, no systematic investigation of these aspects and their effects on the crustal thickness and surface age of Venus has been performed. We thus build on the work of Rolf et al. (2018) and address the following questions: (1) How do episodic overturns affect the evolution and resurfacing history of Venus? (2) What controls the timing, duration, and frequency of overturn events? (3) Do overturn events facilitate the generation of a young surface such as inferred from Venus's cratering statistics? (4) Can parts of the surface resist recycling during overturn events? To address these questions, we introduce our methodology and diagnostics in Section 2, present our results in Section 3, and discuss these in the context of Venus in Section 4 to support a number of key conclusions (Section 5).

2. Methodology

2.1. Physical Model

We compute the thermochemical evolution of Venus's interior in a 2D spherical annulus using the mantle convection code StagYY (Tackley, 2008). The model setup is similar to that in Rolf et al. (2018), which itself is based on Armann and Tackley (2012). Its most important features are the strongly temperature-, pressure- and stress-dependent viscosity, major mineral phase transitions and partial melting (see subsequent paragraphs and the papers cited above for more details).

We solve the governing equations arising from the conservation of mass, momentum, and energy in the extended Boussinesq approximation. This approximation includes the terms for viscous dissipation and adiabatic heating in the heat transport equation and therefore improves consistency of the governing equations in the presence of latent heat effects related to phase transitions and partial melting (Christensen & Yuen, 1985). This implies that an adiabatic temperature gradient is included in the modeled temperature fields. With our assumed model parameters (Table 1), the adiabatic temperature increase is ~850 K across the whole mantle.

2.1.1. Viscosity

In our models, effective mantle viscosity (η) is an average of two contributions. The first one accounts for viscous deformation and is computed using Arrhenius' law:

$$\eta_1 = A\eta_0\eta_p \exp\left(\frac{E_A + pV_A}{R_g T}\right).$$

Here, A is a pre-factor that forces η_1 to be equal to the reference viscosity η_0 at reference pressure ($p = 0$ Pa) and reference temperature ($T = 1613$ K). R_g is the gas constant, E_A the activation energy, and V_A is the activation volume, which depends on pressure according to $V_A(p) = V_{A0} \exp(-p/p^*)$ (Tackley et al., 2013). In this equation, V_{A0} is the activation volume at $p = 0$ Pa and $p^* = 400$ GPa is a scaling pressure, which determines the decrease of activation volume toward the lower mantle. Our employed value of activation energy leads to a strong thermal viscosity variation that results in the formation of a stagnant lid at the top of the mantle, which does not actively participate in the convection of the mantle. Still, our chosen value is likely lower than for real rocks, but we made this choice as a compromise between realism and computational feasibility. Moreover, viscosity in our model is a posteriori limited to the interval (10^{18}–10^{25}) Pa s.

Table 1
Physical Parameters and Symbols

Physical parameters	Symbol	Value	Dimension
Planetary radius	R_s	6.052×10^6	m
Core radius	R_c	3.186×10^6	m
Mantle thickness	D_0	2.866×10^6	m
Surface temperature	T_s	740	K
CMB temperature	T_c	3870	K
Superadiabatic temperature drop	ΔT_S	2300	K
Gravitational acceleration	g_0	8.87	m s^{-2}
Internal heating rate	H_p	5×10^{-12}	W kg^{-1}
Mantle density	ρ_0	3,378	kg m^{-3}
Mantle thermal expansivity	α_0	2×10^{-5}	J mol^{-1}
Mantle thermal conductivity	k_0	4	W m^{-1}K^{-1}
Activation energy	E_A	2×10^5	J mol^{-1}
Activation volume	V_{A0}	3.5×10^{-6}	m^3 mol^{-1}
Mantle specific heat capacity	C_{p0}	1,250	J kg^{-1} K^{-1}
Latent heat of melting	L_m	6×10^5	J kg^{-1}
Clapeyron slopes (ol system)	$\gamma_{ol\,(730/450)}$	$(-2, 2) \times 10^6$	Pa K^{-1}
Clapeyron slopes (px system)	$\gamma_{px\,(800/450/65)}$	$(1, 1, 0) \times 10^6$	Pa K^{-1}
Density jumps (ol system)	$\Delta\rho_{ol\,(730/450)}$	(150, 250)	kg m^{-3}
Density jumps (px system)	$\Delta\rho_{px\,(800/450/65)}$	(150, 150, 250)	kg m^{-3}

The term η_p describes the modulation of viscosity due to different mineral phases. It has been shown, however, that a significant viscosity discontinuity at the boundary between upper and lower mantle phases deteriorates the match between the model-predicted and the observed correlation between Venus's surface topography and geoid (Rolf et al., 2018). While this may be an effective response from a combination of several processes, we take this as a motivation to use $\eta_p = 1$ in this work, for simplicity. We emphasize that viscosity still varies significantly with depth due to the pressure dependence using a finite activation volume. The typical viscosity variation between upper- and lowermost mantle is a factor of ~100. A radial viscosity variation has a strong impact on topography and geoid and as shown by Steinberger et al. (2010) and Rolf et al. (2018); the effective viscosity contrast between upper and lower mantle results in a rather good match between model predicted and observed surface geoid. In our 2D model, analyzing topography and geoid patterns is not too meaningful, but we confirmed that our models at least predict topography and geoid ranges that are consistent with Venus's present-day observations (see Figure S1). As an additional detail, our models also predict the high correlation between topography and geoid, at least at long-wavelength, which is characteristic of Venus. We therefore have confidence that our modeled viscosity structure is reasonable for Venus.

In our computed stagnant lid evolutions (see Table 2), η_1 is used as the effective viscosity entering the governing equations. We also consider evolutions featuring global overturn episodes in which a weakening mechanism is required in the lithosphere. Here, we assume this to be plastic yielding. As long as convective stresses remain below a critical value (the yield stress, σ_Y) material deforms viscously, but once σ_Y is reached deformation becomes plastic. The yield stress is given by Byerlee's law $\left(\sigma_Y = \sigma_0 + \mu p\right)$ using a friction coefficient of $\mu = 0.5$. The surface value $\left(\sigma_0\right)$ describes the cohesion of the material and is used here as a tuning

Table 2
List of Performed Computations and Their Governing Parameters, Reference Viscosity, η_0 in Pa s and, for the Episodic Cases, the Surface Yield Stress (σ_0)

Model name	η_0 (Pa s)	σ_0 (MPa)
S1e20	1.e+20	-
S2e20 (3D)	2.e+20	-
S3e20 (*)	3.e+20	-
S1e21	1.e+21	-
S2e21	2.e+21	-
S3e21	3.e+21	-
S1e22	1.e+22	-
E50_1e20	1.e+20	50
E50_2e20 (3D)	2.e+20	50
E50_3e20 (*)	3.e+20	50
E50_1e21	1.e+21	50
E40_3e20	3.e+20	40
E45_3e20	3.e+20	45
E55_3e20	3.e+20	55
E65_3e20	3.e+20	65
E70_3e20	3.e+20	70
E80_3e20	3.e+20	80
E90_3e20	3.e+20	90
E100_3e20	3.e+20	100

Note. Model names are constructed as follows: the initial capital letter denotes the tectonic regime, S for stagnant, E for episodic. In the latter set, the numeric part after the initial letter denotes the value of σ_0. The second part of the model name indicates the reference viscosity in Pa s. Two cases, marked "(3D)," where run in 2D and in 3D geometry for comparison. The suffix "(*)" indicates that a case has been recomputed with several values of melt eruption efficiency (see Supporting Information S3).

variable to modulate the occurrence and frequency of overturn episodes (i.e., we do not claim that our model values are realistic for the rocks found on Venus's surface).

2.1.2. Composition and Mineralogy

The initial mantle material is a mixture of harzburgite and basalt, which consist of 75% olivine (ol) + 25% pyroxene-garnet (px) and 0% ol + 100% px, respectively (see Xie & Tackley, 2004). The ol- and px-systems undergo phase transitions at different depths (ol: 450 and 730 km; px: 65, 450, and 800 km). These depths are scaled from the Earth, accounting for the somewhat lower gravity and thus pressure at a given depth on Venus. Phase transitions related density jumps and Clapeyron slopes are specified in Table 1. As pointed out in the previous section, we do not consider an additional viscosity contrast associated with these phase transitions.

Initially, composition is homogeneous throughout the mantle, but when the local temperature exceeds the solidus partial melting occurs and leads to local compositional variations (Nakagawa et al., 2009; 2010; Xie & Tackley, 2004). Partial melting consumes latent heat; moreover, the molten material is assumed to be strongly buoyant and to rise to the surface on time scales much shorter than typical for solid-state convection. For a first-order description, the melt is thus instantaneously extracted from the mantle and emplaced as crust at the top of the mantle, which is a parametrization for eruptive volcanism (Keller & Tackley, 2009). Only basaltic melt in the upper mantle ($d < 730$ km) is extracted, while it would be left if occurring in the lower mantle (very atypical). In reality, the depth layer over which basaltic melt is buoyant is confined to shallower depth. However, Armann and Tackley (2012) have shown that limiting the maximum depth of melt extraction to 300 km does not greatly impact the results, which we also observed in this study. Our assumed solidus curve increases more strongly with depth than the typical temperature profile observed in our model, so that the actual degree of melting below 300–400 km depth is actually very small (if any).

For simplicity, we assume that all the locally molten material is extracted and erupted (i.e., the melt eruption efficiency is $\varepsilon = 100\%$). This is clearly an end-member scenario since in reality significant parts of the melt do not reach the surface, but form magmatic intrusions. Recently, planetary evolution models featuring coexisting eruptions and intrusions have been formulated (Lourenço et al., 2018; Rozel et al., 2017), but our model does not yet allow for this complexity (see Supporting Information S3 and discussion in Section 4). The mantle below the emplacement depth is compacted accordingly to maintain conservation of mass. Maximum melt fractions largely remain below 40%, so below the threshold above which effective viscosity decreases dramatically as interconnectivity of the solid matrix is lost (Abe, 1995).

Only the basalt fraction of the mantle material can melt, so that the emplaced crust is basaltic. The solidus considered here is taken from previous studies and is parametrized based on experimental data from Earth's mantle rocks (see Xie & Tackley, 2004). Becoming depleted in basalt, material becomes more difficult to melt, which is considered here by a linear increase in the solidus temperature by up to 150 K. All information related to material composition is tracked by tracer particles that are distributed over the entire mantle and advected by the mantle flow. The resulting material composition at any given location in the model is computed from the tracer distribution using the tracer ratio method (Tackley & King, 2003).

Table 3
Diagnostics for All Stagnant Lid Models Discussed in Section 2.4: Mean Crustal Thickness, $\delta_{cr} \pm \sigma_{cr}$; Mean Surface Age, $\mu_{sa} \pm \sigma_{sa}$; Ratio of Total Cumulative Mass of Erupted Material to the Total Mantle Mass, E_m/M_m

Model	$\delta_{cr} \pm \sigma_{cr}$ (km)	$\mu_{sa} \pm \sigma_{sa}$ (Gyr)	E_m/M_m (-)	ϕ_s (mW m^{-2})
S1e20	98 ± 17	0.11 ± 0.09	0.36	29 ± 0.8
S2e20	113 ± 18	0.12 ± 0.08	0.29	23 ± 0.3
S3e20	124 ± 20	0.11 ± 0.08	0.27	22 ± 0.1
S1e21	140 ± 10	0.18 ± 0.13	0.17	19 ± 0.7
S2e21	188 ± 15	0.14 ± 0.10	0.13	15 ± 0.6
S3e21	200 ± 17	0.16 ± 0.12	0.14	13 ± 0.9
S1e22	198 ± 72	0.27 ± 0.21	0.12	11 ± 0.5

Note. This diagnostic is given after 4.4 Gyr of evolution at which time most cases have reached a state close to equilibrium, ϕ_s is the average surface heat flux observed at 4.4 Gyr. If given, ± symbols indicate one standard deviation.

2.2. Initial and Boundary Conditions

We use a 2D spherical annulus geometry (Hernlund & Tackley, 2008) with a grid resolution chosen after a consideration from three sample resolutions (1024 × 128, 768 × 96, and 512 × 64). Out of these three, not much deviation in the final output was observed, and as a compromise between accuracy and computational cost we chose the intermediate resolution. The radial grid spacing is refined at the surface, phase transitions, and above the CMB. We use 7.28 million tracers to track composition (∼100 tracers per cell on average). The model employs free-slip and isothermal boundaries at the surface and CMB. The surface temperature is the one inferred for present-day Venus (740 K). At the CMB, we impose a temperature of 3870 K, which reflects the hot end-member scenario of Dumoulin et al. (2017), but we note that this parameter is very uncertain for Venus and even for the Earth. We do not consider changes in these boundary temperatures with time (Gillmann & Tackley, 2014), because we are mostly interested in the system behavior in a statistically steady state, which is difficult to achieve using these complexities. This is also consistent with our assumption of a time-independent internal heating rate ($H_p = 5 \times 10^{-12}$ W kg^{-1}), which should also decay with time in a more realistic model. A discussion on the potential role of different internal heating rates is provided in Section 4.3. Internal heat sources are distributed evenly across the mantle.

The initial temperature field is adiabatic with potential temperature set at 1900 K and with a boundary layer thickness of 80 km at top and bottom of the model domain. Convective instability is initiated by superimposing random perturbations with an amplitude of 20 K upon the initial temperature field. The initial conditions for Venus's evolution are not known and can affect the resulting tectonic regime (e.g., King, 2018; O'Neill et al., 2016) and across our suite of simulations (see Section 2.3) we did not test different initial conditions. However, it is important to point out that the goal of our study is not to examine under which conditions one (or another) geodynamic region develops, but to explore how the developed regime affects the geodynamic diagnostics listed in Section 2.4.

2.3. Computed Simulations

We present 21 numerical simulations (see Table 2), eight cases in stagnant lid (S*), and 13 in episodic lid regime (E*). The nominal integration time is set to 4.4 Gyr, but is extended if the evolution has not reached a statistical steady state by then. The nominal choice approximately matches the entire duration of Venus's evolution, but this has no physical significance here.

In our set of simulations, we varied the reference viscosity (η_0) between 10^{20} and 10^{22} Pa s and the surface yield stress (σ_0) between 40 and 100 MPa. These absolute values of σ_0 are chosen to enable an evolution with episodic overturns, they should not be seen as a constraint on Venus's unknown lithospheric strength. Instead, we rather want to derive systematics in the style and frequency of overturns with varying yield stress. We do not investigate the yield stress dependence of the transition between episodic and stagnant regime, which is affected by many parameters fixed here and also by boundary and initial conditions. In stagnant-lid cases, no yield stress is considered, so that the development of a stagnant-lid is predefined and independent of the chosen initial conditions for instance.

2.4. Diagnostics

We extract several diagnostics (listed in Tables 3 and 4), which are derived and displayed with the post-processing tool *StagLab* (Crameri, 2017, 2018). Since we are interested in the surface responses of interior dynamics, we focus on the (mean) surface age (μ_{sa}) and (mean) crustal thickness (δ_{cr}). In order to characterize the evolution of magmatism and volcanism, we also compute the total (cumulative) mass of erupted material, normalized to the mass of the mantle (E_m/M_m). This diagnostic gives insight into the strength of

Table 4
Diagnostics for All Episodic Lid Models as Discussed in Section 2.4: Mean Crustal Thickness, $\delta_{cr} \pm \sigma_{cr}$, for Either Just Before the Beginning (B_{OT}) or Just After the End of the Overturn Event (P_{OT}); Mean Surface Age, $\mu_{sa} \pm \sigma_{sa}$; Ratio of Total Cumulative Mass of Erupted Material to the Total Mantle Mass, E_m/M_m; Number of Overturns N_{OT}; Average Duration of the Overturns t_{OT}; the Average Duration of Tectonic Quiescence Between Overturn Events, Δt_{OT}. $\phi_{s_}$min is the Average Surface Heat Flux Observed Between the Overturn Events and $\phi_{s_}$max is the Average Surface Heat Flux During the Overturn Events

	$\delta_{cr} \pm \sigma_{cr}$ (km)		$\mu_{sa} \pm \sigma_{sa}$ (Gyr)						ϕ_s (mW m^{-2})	
Model	B_{OT}	P_{OT}	B_{OT}	P_{OT}	E_m/M_m	N_{OT}	t_{OT} (Gyr)	Δt_{OT} (Gyr)	Min	Max
E50_1e20	39 ± 15	30 ± 14	0.19 ± 0.10	0.04 ± 0.06	0.18	7	0.15 ± 0.09	0.3	24	79
E50_2e20	50 ± 22	32 ± 22	0.26 ± 0.14	0.14 ± 0.06	0.15	4	0.21 ± 0.03	0.14	25	65
E50_3e20	55 ± 20	25 ± 12	0.34 ± 0.13	0.20 ± 0.10	0.14	3	0.37 ± 0.10	0.43	24	68
E50_1e21	37 ± 17	32 ± 15	0.46 ± 0.34	0.22 ± 0.20	0.11	*n*	-	-	22	52
E40_3e20	39 ± 15	32 ± 15	0.37 ± 0.18	0.12 ± 0.17	0.15	*n*	-	-	24	66
E45_3e20	62 ± 23	34 ± 14	0.40 ± 0.08	0.09 ± 0.07	0.15	3	0.34 ± 0.20	1.06	24	65
E55_3e20	36 ± 24	28 ± 14	0.34 ± 0.18	0.09 ± 0.07	0.14	3	0.38 ± 0.02	1.25	24	60
E65_3e20	69 ± 27	30 ± 18	0.25 ± 0.13	0.05 ± 0.04	0.13	3	0.30 ± 0.08	0.76	19	70
E70_3e20	55 ± 23	30 ± 20	0.24 ± 0.13	0.08 ± 0.06	0.13	3	0.15 ± 0.02	1.00	18	78
E80_3e20	125 ± 25	30 ± 14	0.11 ± 0.06	0.04 ± 0.02	0.14	1	0.36	-	19	79
E90_3e20	126 ± 32	49 ± 47	0.10 ± 0.05	0.04 ± 0.05	0.13	1	0.08	-	19	77
E100_3e20	126 ± 30	26 ± 14	0.09 ± 0.05	0.05 ± 0.04	0.13	1	0.45	-	18	76

Note. If given, ± symbols indicate one standard deviation. The indicator "*n*" is used where the number of overturns is more than 3–5 Gyr^{-1}, which almost resembles a continuous mobile lid regime.

volcanic activity in a time-averaged sense; the higher the diagnostics is after a given time span, the more volcanism has occurred. In episodic cases, we additionally compute the number of overturn events (N_{OT}) as well as their spacing (Δt_{OT}) and duration (t_{OT}).

2.4.1. Surface Age

Surface age is an important constraint on Venus's surface evolution and has been inferred from the crater statistics of geological units observed on Venus (Kreslavsky et al., 2015). So far only very limited attempts (see Noack et al., 2012; Rolf et al., 2018) used surface age distributions as a constraint for dynamic evolution models, which we take as a motivation to investigate it more rigorously. In our models, surface age is tracked as the residence time of tracer particles in the uppermost layer of the numerical grid. All other tracers outside this top layer carry an undefined surface age. Typically, many tracers are present in each grid cell, so that there may be some age stratification within the cell, but our model cannot capture such sub-grid scales. We thus take the mean of all tracer surface ages as a characteristic value for the entire cell and define this as the age of the related patch of surface area. As melt reaches the surface, the tracer particles carried by the melt are considered as long as they reside in the topmost cells. In the stagnant lid regime, molten tracers may reach the surface by melt extraction equivalent to volcanism. No large-scale surface recycling is possible in this mode, so the only way to remove a tracer from the shallowest level is by addition of new material on the surface. This pushes older material downwards, eventually deep enough so that delamination processes transport it further down. In cases with lithospheric overturn, tracers may reach the surface either via melt extraction or tectonically in situations where the surface is mobilized (like during seafloor spreading on Earth). Similarly, the tracers get recycled into the deeper interior during overturn episodes (like during terrestrial subduction).

We note that melting and thus eruptive volcanism is a local process often happening on the scale of individual grid cells. This can cause strong lateral variations over short length scales. In reality, the distribution of lava may be smoother since lava will flow laterally following the topographic gradients on the planetary surface until solidification. Capturing this is currently beyond the capacity of our approach. We thus mostly focus on the mean surface age (μ_{sa}) and its standard deviation (σ_{sa}) in our discussion, which can be related to Venus's mean surface age as inferred from cratering statistics, respectively.

2.4.2. Crustal Thickness

The thickness of Venusian crust is not directly observed, given the lack of seismic measurements for instance. Its lateral variations may be inferred from the observed gravity and topography (Anderson & Smrekar, 2006; James et al., 2013; Jiménez-Díaz et al., 2015; Wieczorek, 2007), but typically this requires an assumption on the mean thickness, which is only nonuniquely determined from surface topography and gravity. Consequently, our models add independent insight by deriving crustal thickness consistent with the internal evolution.

In our model, crustal thickness is equivalent to the layer of basaltic material that is emplaced at the surface as a consequence of volcanism. This layer thickness is tracked in each radial column of the numerical grid following Keller and Tackley (2009). Due to the initial condition with homogeneous composition in our model, the crustal thickness is initially zero, until the onset of melting. As for the surface age diagnostic, we mostly focus here on the mean value and its standard deviation, but we will also touch upon lateral variations and their link to internal dynamic features.

3. Results

We first discuss two reference cases: one stagnant-lid case (S3e20) and one episodic case (E50_3e20). Both cases differ only in terms of the yield strength, which is infinite in the former and finite in the case.

3.1. Stagnant Lid Evolution

3.1.1. General Characteristics

In the stagnant-lid reference case S3e20 (Figure 1a), the average potential mantle temperature gradually increases from its initial value due to the dominance of internal heating, reaching a maximum at ~1.7 Gyr. The mantle temperature then gradually decreases at a rate of 15–20 K Gyr^{-1} until an equilibrium is reached. The mean temperature is roughly 2300 K during at least the final billion year of evolution, when internal heat generation and surface heat loss are in balance. We define this period as the equilibrium state.

Since the lithosphere is immobile, heat can only escape via conduction and volcanism through melt extraction, which appears inefficient and explains the small heat flux of only ~22 mW m^{-2}, a factor of 4–5 less than the terrestrial value (Figure 1b), but similar to other model predictions (e.g., Reese et al., 2007). In contrast, the heat flux across the bottom boundary of the mantle adjusts relatively quickly into an equilibrium state (~74 mW m^{-2}, Figure 1c). This gives rise to the formation of several plumes at the CMB (Figure 2). The number of plumes slowly decreases until an equilibrium state with three plumes is established. The system remains weakly time-dependent, but the general structure is maintained (compare Figures 2h and 2j). Finally, the plumes appear most prominent in the lower mantle, but less so in the upper mantle. The total temperature field is not a complete representation of the strength of the plume in our model, because during a plume's rise through the mantle its absolute temperature reduces due to adiabatic decompression. Indeed, subsequent analysis shows that there is still magmatism and thus melt eruption at the surface in the regions above active plumes. It is, however, evident that these plumes are not strong enough to pierce through an intact, stable, and strong lithosphere. Gülcher et al. (2020) suggest that mantle plumes interacting with the lithosphere can lead to domical uplift on Venus, which be the origin of some of the planet's central volcanoes. The lithosphere in our model may be too thick and strong to show such features (see Figure S1), but such regional scales (some hundreds of kilometers) are anyway difficult to analyze in our global models with limited resolution.

With our assumption that the lithosphere cannot yield in the stagnant-lid scenario, subducting slabs that locally cool the mantle are absent. This also prevents efficient crustal recycling and leads to larger amounts of depleted mantle, because the once extracted basalt components are difficult to mix in again. During the evolution, partial melting and thus eruptive volcanism happen continuously except for the very early phases during which the evolution is affected by the initial condition. The rate of volcanism evolves slowly and is linked to the temperature in the mantle. The maximum rate (which corresponds to the maximum slope in the evolution of cumulative erupted mass, Figure 1d) is obtained between ~1.7 and 2.5 Gyr, when the mantle is also at its hottest state. Once thermal equilibrium is reached, the rate of eruption is essentially constant.

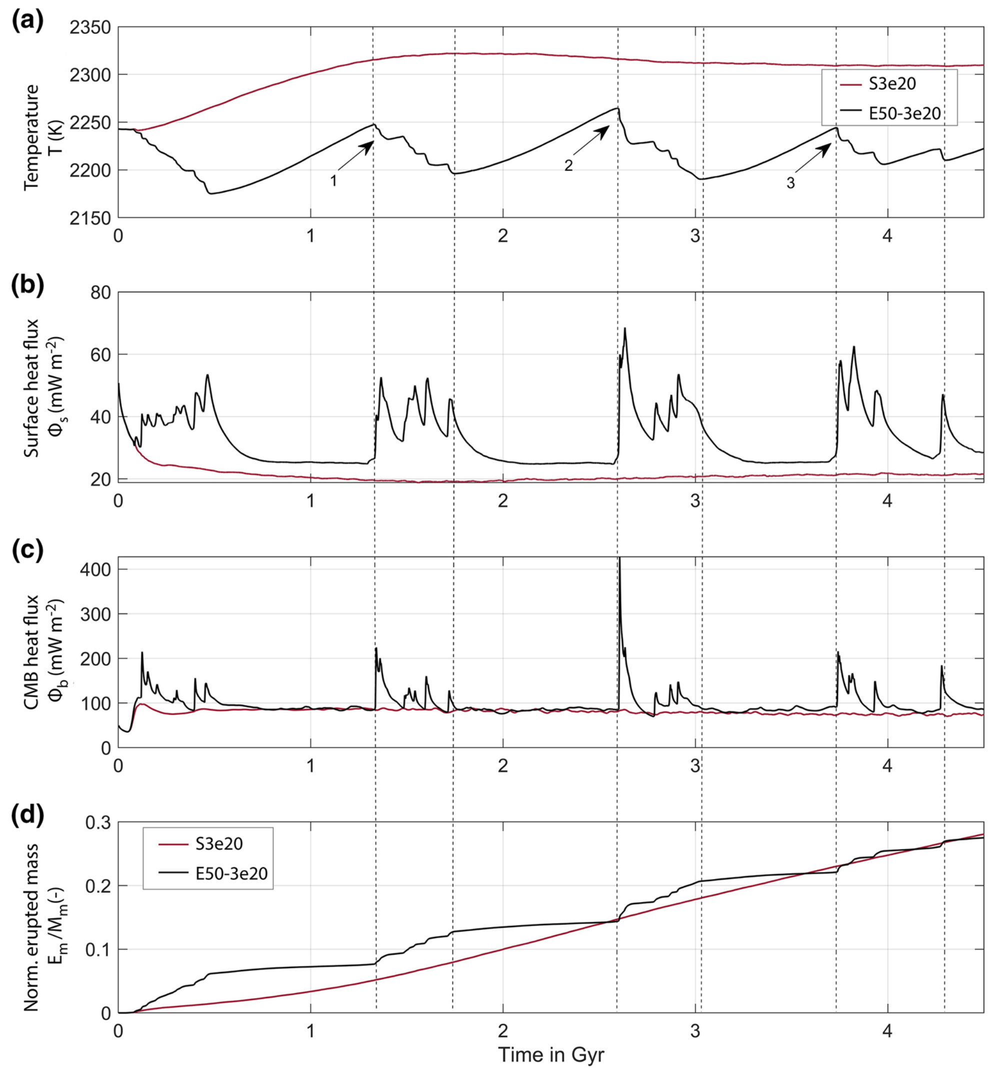

Figure 1. Evolution of cases S3e20 and E50_3e20. Shown are (a) globally averaged temperature, (b) average heat flux across the surface, (c) average heat flux across the core-mantle boundary, and (d) total mass of erupted material (E_m, cumulative over time) normalized to the total mass of the mantle (M_m). The dashed lines mark the overturn periods in the episodic cases, whose onsets are indicated with arrows in panel (a).

The continuous melt extraction thickens the crust with time leading to an equilibrium thickness of ~120 km (Figures 3c–3g). Such a thick crust easily extends into the stability field of eclogite (below 65 km here), which is denser than the shallower basalt. This induces significant negative buoyancy and stress into the lithosphere, which would likely fail under these stresses, if it was not prohibited in the stagnant-lid scenario. Since magmatism and volcanism are ongoing throughout the entire evolution, one may then expect continuous growth of the crust with time. An equilibrium thickness is still reached, because convective erosion and dripping can recycle the deeper, mostly eclogitic parts back into the mantle (Armann & Tackley, 2012). However, these processes seemingly become effective only below the thermal boundary layer in which the relatively low temperature causes high viscosity that inhibits viscous recycling processes at shallower depth, even though the eclogitized crust is negatively buoyant.

The influence of plumes, and the magmatic activity related to them, shows a clear imprint on crustal thickness (Figures 3c–3g). In the early stages of evolution, when the mantle is still heating up globally (Figure 1a), the effect of plumes is most pronounced since they are the only regions inducing substantial melting, while the rest of the upper mantle is not yet hot enough to do so (Figure 2c). Later in the evolution,

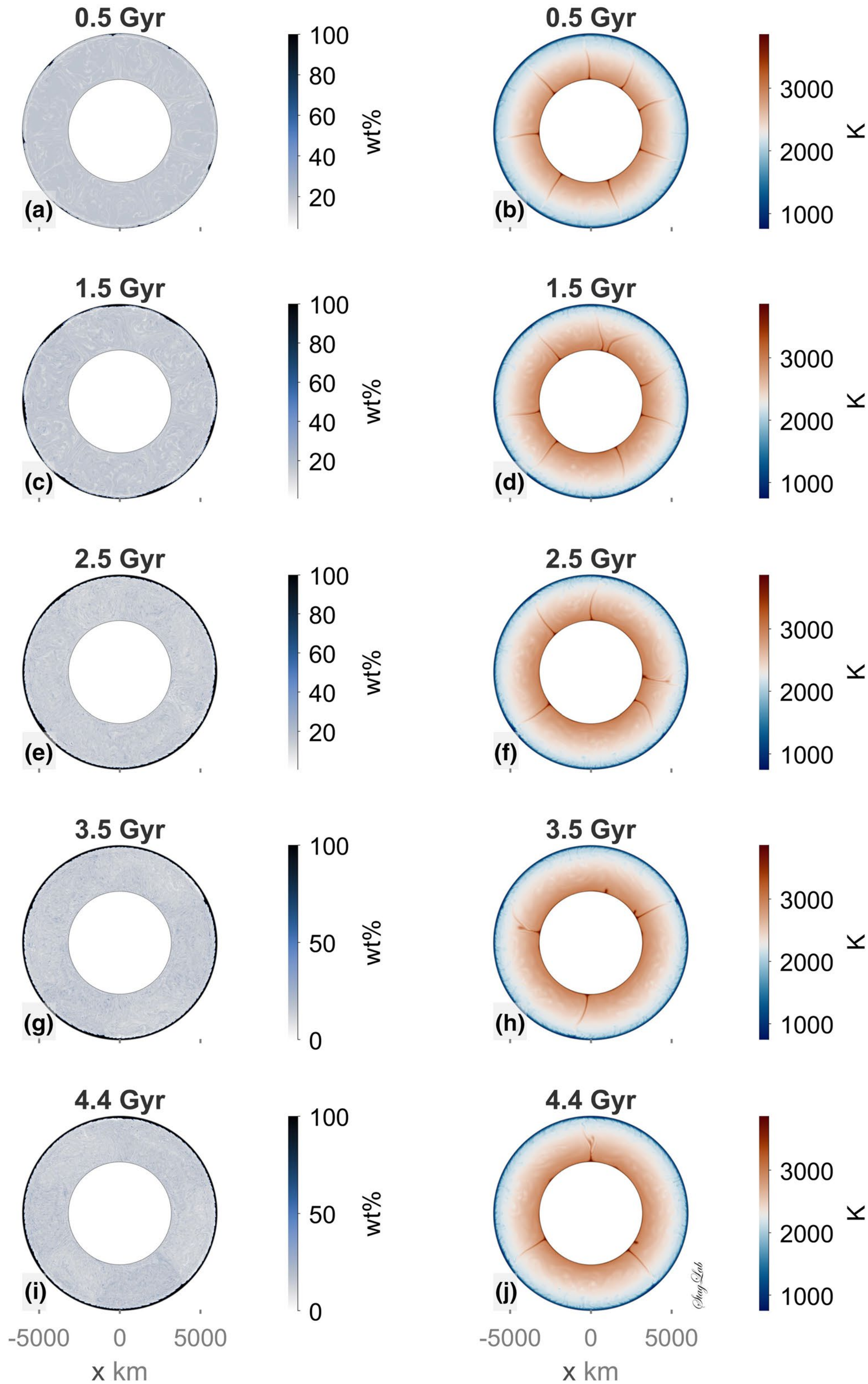

Figure 2. Evolution of basalt fraction (100% = pure basalt, 0% = no basalt) and mantle temperature for case S3e20 for different points in time as indicated.

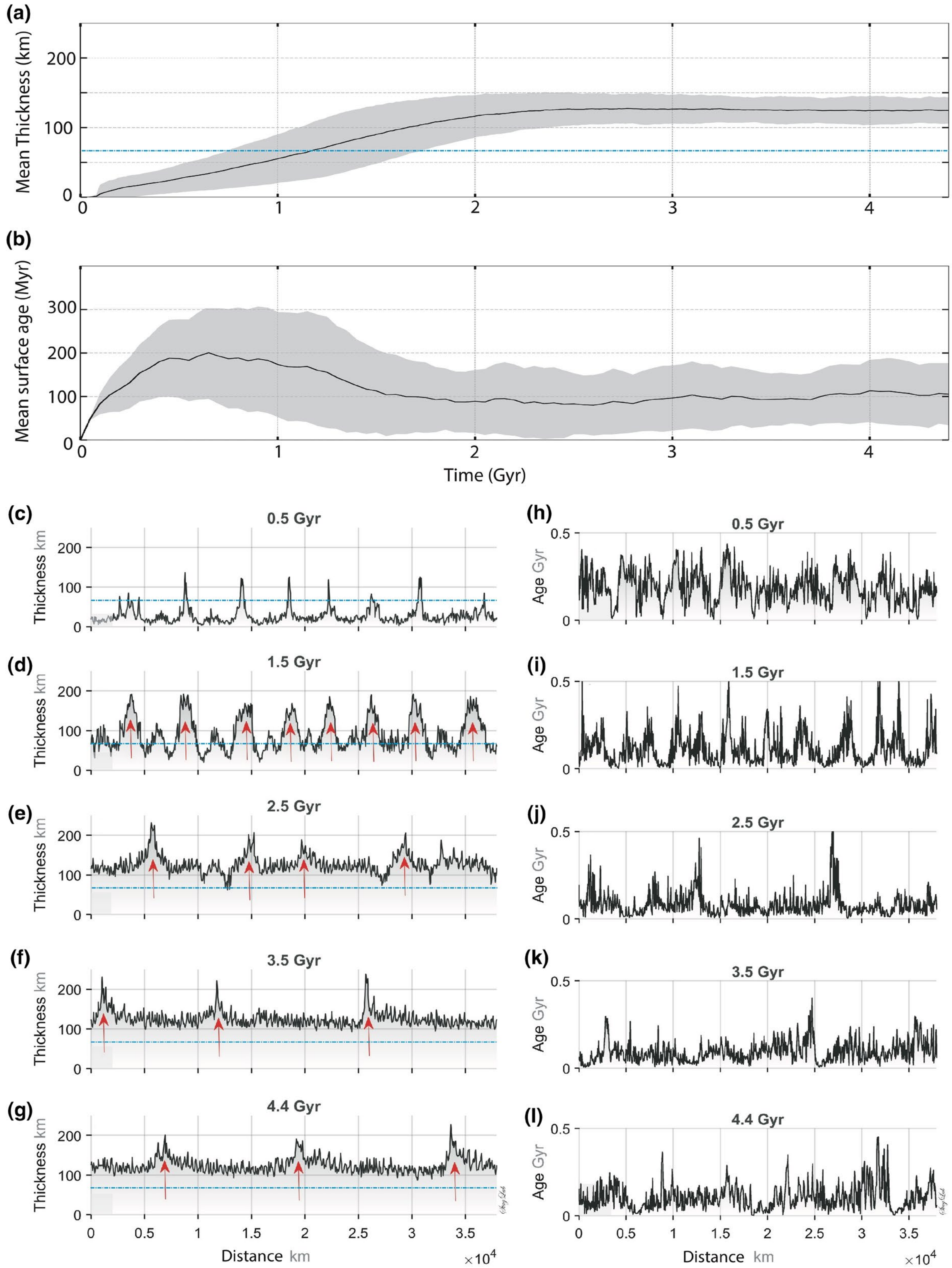

Figure 3. Temporal evolution of (a) mean crustal thickness and (b) mean surface age in case S3e20. Panels (c–l) show the lateral variations of crustal thickness (left) and surface age (right) at different times. The plume locations are indicated by red upward arrows and the *x*-axis shows the horizontal distance across the surface measured starting from six o'clock along the spherical annulus in Figure 2 in clockwise direction. The horizontal dash-dotted line in the panels for crustal thickness indicates the transition of basaltic material into eclogite.

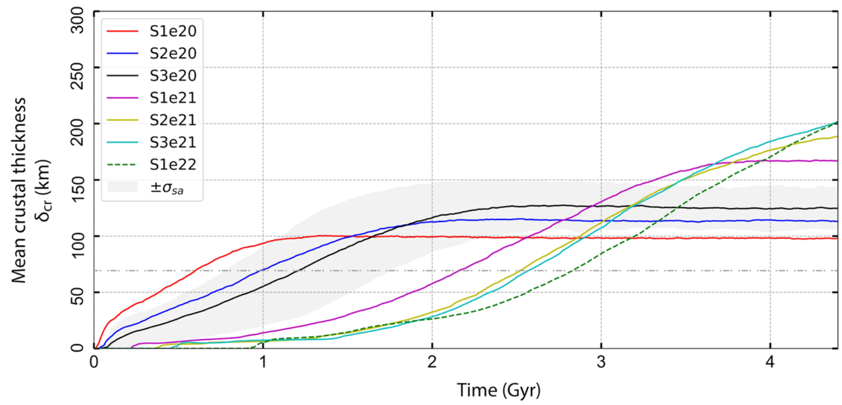

Figure 4. Evolution of crustal thickness in stagnant lid cases with varying reference viscosities and the respective color shade region indicate the $\pm 1\sigma$ standard deviation of the correspondingly to the reference stagnant lid case S3e20 (reference viscosity, $\eta_0 = 3 \times 10^{20}$ Pa s). The horizontal dash-dotted line indicates the transition depth into dense eclogite (~66 km).

when an equilibrium state has developed, the effect can still be observed, but the differences in crustal thickness above plumes compared to the background level are smaller (Figures 2e–2g).

Accordingly, the mean surface age increases quickly during the initial 0.5 Gyr of evolution without extensive volcanism (Figure 3b). Once approaching equilibrium, the surface adopts a very young mean age of only ~100 Myr, but lateral variations are quite large and the surface age ranges from 50 Myr to up to 300–400 Myr (e.g., Figure 3l). The surface age distribution is linked to crustal thickness since the youngest surface appears atop the hot mantle plumes, which are also the regions in which the thickest body of crust has accumulated (Figures 3h–3l). Note that this relation may be a result of the here-assumed purely extrusive magmatism. In reality, volcanic resurfacing could be hindered by a thick crust in which magmatic intrusions are more likely to form. Also, the crust may not ever become so thick with intrusions happening (see Section 4.1 and Lourenço et al., 2018). In our model though, the oldest regions exceeding a surface age of 300 Myr or so make only a small fraction of the distribution. Our reference stagnant lid model thus predicts a very young mean surface age (i.e., 100 ± 90 Myr). The observed trends are relatively robust against the varied parameters in our model, but detailed timescales and equilibrium values are of course affected, which we discuss in the subsequent sections.

3.1.2. Influence of Reference Viscosity (η_0)

Previous studies (Armann & Tackley, 2012; Keller & Tackley, 2009; Lourenço et al., 2016) suggest that increasing viscosity (here, η_0) would lower the convective heat transport causing more melting at depths and leading to thicker crust. In higher viscosity cases, the maximum crustal thickness is achieved after a longer time, whereas it occurs earlier in lower viscosity cases. This is due to the initial high convective heat transport in the low viscosity cases that quickly cools the mantle leading to less melt generation later. With higher reference viscosity, the evolution is affected longer by its initial condition and it generally takes longer to reach the equilibrium state in which our diagnostics do not follow a pronounced trend anymore. For example, in our cases with higher reference viscosity more than 4.4 Gyr integration time are needed until crustal thickness reaches an equilibrium (Figure 4); in these cases, we extended the model time to obtain the equilibrium value, which is plotted in Figure 5.

If the reference viscosity is sufficiently low (e.g., in case S1e20 with $\eta_0 = 10^{20}$ Pa s), the initial phase of globally heating the mantle as observed in the reference case vanishes from the evolution and temperature decreases right from the initial time until an equilibrium is reached, because surface heat loss is immediately large enough to counterbalance radiogenic heating. This is also reflected in the fastest mantle cooling rate, the highest surface heat flux, and the largest amount of cumulative erupted material (Table 3). However, even with the lowest reference viscosity, the average surface heat flux does not exceed 30 mW m^{-2} (Table 3); with high reference viscosity, it can be as low as 11 mW m^{-2}. Such values are comparable to those obtained in Reese et al. (2007) and clearly indicative of a long-term stable stagnant lid.

10.1029/2019JE006258

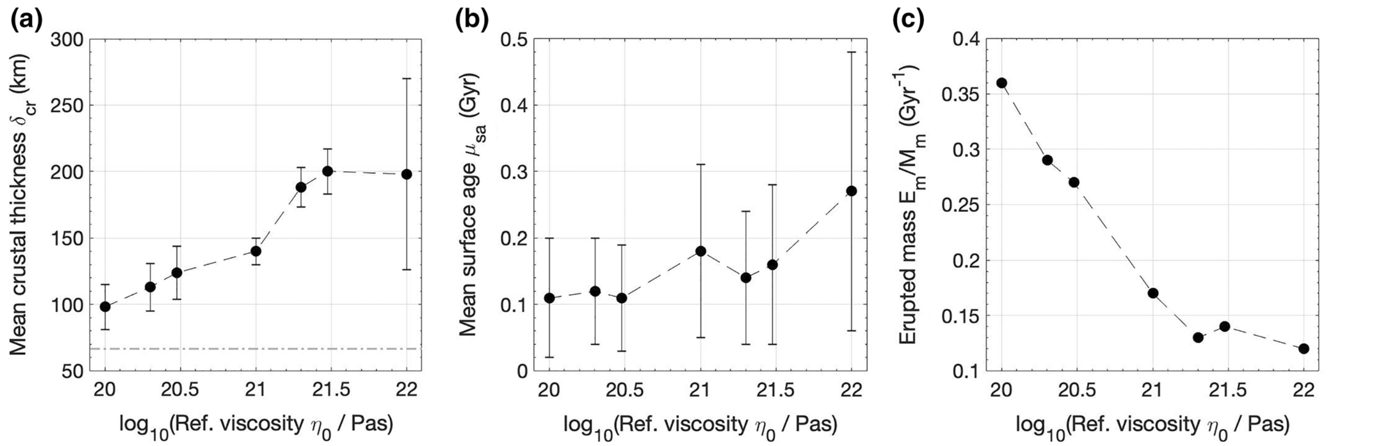

Figure 5. (a) Equilibrium mean crustal thickness, (b) equilibrium mean surface age, and (c) normalized mass of erupted material after 4.4 Gyr, plotted as a function of reference viscosity (η_0). Error bars denote the respective standard deviation. The horizontal dash-dotted line indicates the transition depth into dense eclogite.

As a first-order trend, equilibrium crustal thickness increases with increasing reference viscosity (Figure 5a). This is observed although the amount of erupted material is decreased (Table 3), which means that lower reference viscosity leads to more efficient recycling at the crustal base as the thermal boundary layer is thinner and convective velocities are higher. However, even in the lowest viscosity case tested here, the observed equilibrium thickness does not fall below ~100 km. The equilibrium value is reached rather quickly for models with low reference viscosities (Figure 4), but it is not reached at the end of the computation for models with the highest reference viscosities, so that the mean values for these cases (Figure 5a) have to be interpreted with care and may underestimate the true equilibrium value to some degree. It is clear though that a trend exists toward increasing mean crustal thicknesses with higher reference viscosities.

As a general trend, surface age increases with increased viscosity, similar to crustal thickness (Figure 5b). The reason for this is again tied to the thicker thermal boundary layer, which is inefficient in heat transport and leads to less melt eruption as it becomes more difficult to reach the (depth-dependent) solidus in the sub-lithospheric mantle. This effectively limits the rate of volcanic resurfacing (Figure 5c). Comparing the different cases for the surface age variations along the annulus, we observe an increase in standard deviation with increasing viscosity, respectively. The surface is older at thick crustal regions, which hints at slow but continuous magmatism.

To summarize, the higher the reference viscosity, the hotter the interior with thicker crust and the wider the range of ages (Figure 5b), when compared to the lower-to-intermediate reference viscosity. Overall, the mean surface age remains at about ~250 Myr, whereas the upper and lower limits vary for different models.

3.2. Episodic-Lid Evolution

The episodic reference model (case E50_3e20, Figure 1) assumes a surface yield stress of $\sigma_0 = 50$ MPa, which is chosen so that convective stress reaches this value occasionally, plastic yielding can occur and initiate surface mobilization. Over the 4.4 Gyr evolution, overturns are seen temporally set apart in time. The surface mobility (i.e., the ratio between surface velocity to whole mantle velocity, Figure 6a) is high during these episodes, but is close to zero at the remaining times. During the overturn event, substantial resurfacing happens and leads to the recycling of cold surface material into the interior and to net cooling of the mantle (Figure 1a). The previously thick and stable stagnant lid breaks into fragments during the resurfacing events, which allows heat to escape more efficiently. Surface heat flux is strongly enhanced then and gets much closer to the terrestrial value (up to 60–70 mW m^{-2}, Figure 1b). After cessation of an overturn event, it may take several hundred million years for the heat flux to decrease to its pre-overturn level (Figure 1b). Therefore, even if direct measurements of Venus's surface heat flux existed, their interpretation

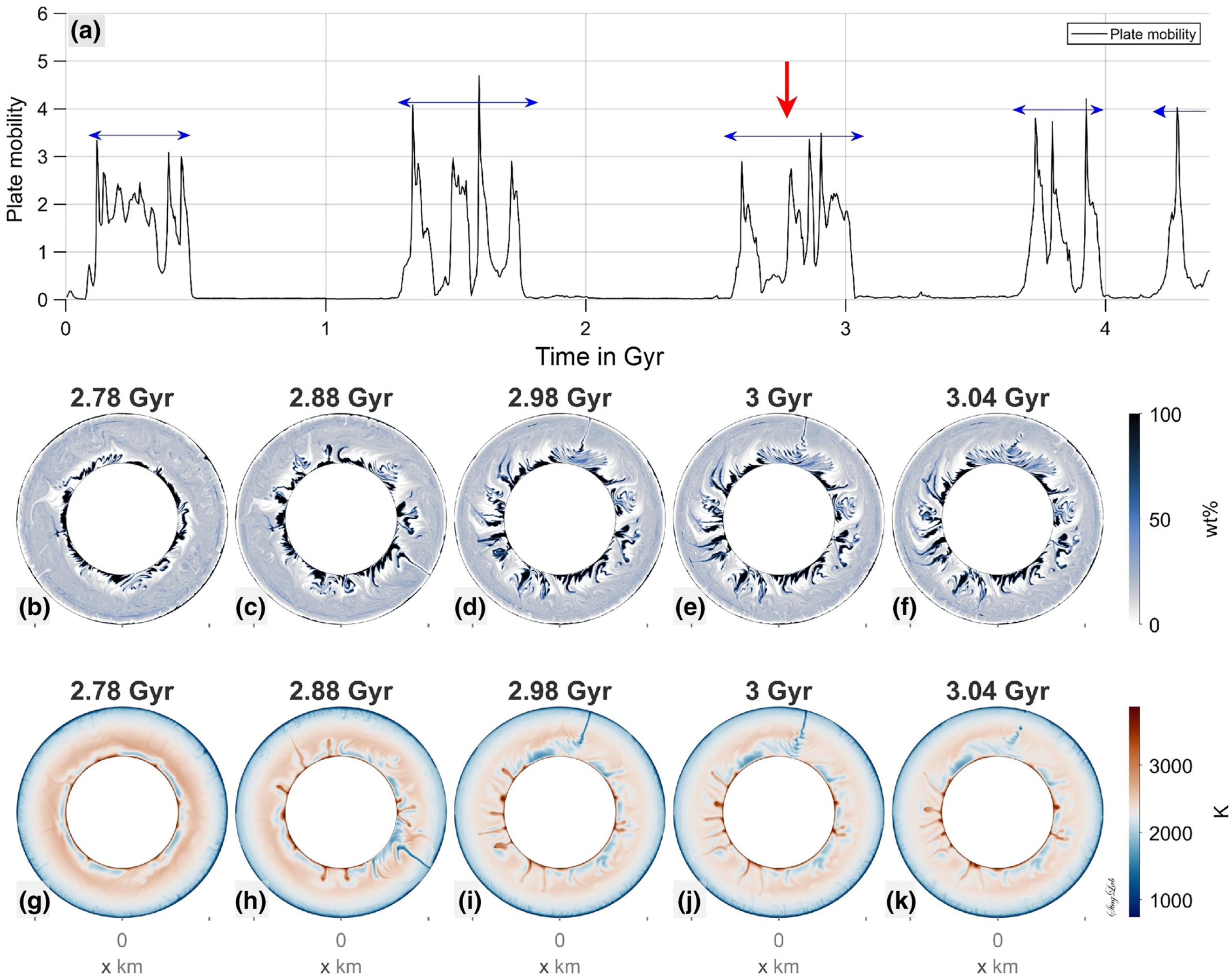

Figure 6. Overturn evolution in case E50_3e20. (a) Evolution of surface mobility. The red arrow indicates the overturn event shown in the snapshots of (b–f) basalt fraction and (g–k) temperature for different points in time. Blue double-arrows denote the duration of overturn events (Δt_{OT}).

with regards to the planets internal structure would require knowledge about the timing and cessation of the latest overturn.

3.2.1. Overturn Dynamics and Episodicity

In this example, several distinct overturn events are observed, which initiate at ~1.28 Gyr, ~2.60 Gyr, and ~3.70 Gyr, each lasting for ~370 ± 140 Myr. The surface is mobile during the overturn episodes and moves with an average velocity that equals or exceeds the interior average velocity (i.e., surface mobility ≥ 1, Figure 6a). Moreover, the time scale of thermal equilibration of the cold recycled material in the interior is typically longer than the time scale of sinking through the mantle. Consequently, cold recycled (basaltic) material can pile up on top of the CMB (Figure 6), where it causes a temporal increase in heat flux (Figure 1c). This material can even form an almost global layer and thereby induce a strong disturbance to the plume pattern established before the overturn (Rolf et al., 2018), but without having a pronounced effects on the center of mass in this spherically symmetric configuration (King, 2018).

The rate of melt production and volcanic activity is not linear in the episodic regime (Figure 1d). During the stagnant-lid phases between the overturns, magmatic activity may almost cease (e.g., between 2.0 and 2.5 Gyr), but during the mobilization events pronounced peaks of volcanic resurfacing occur, so that the total cumulative amount of erupted material is here almost the same in the episodic and the stagnant-lid cases. The pulses in volcanic activity are linked to the recycling of thick lithosphere and crust, which allows hot upper mantle material to reach shallower depth where it is easier to reach the solidus.

3.2.2. Response of Crustal Thickness and Surface Age following Overturn Events

Generally, much thinner basaltic crust is observed in episodic models compared to the stagnant-lid scenario. Lithospheric overturns destroy and recycle thick basaltic provinces and thus reduce the average crustal thickness. Some regions seem to survive one recycling event, but not necessarily multiple ones. In the reference model E50_3e20, we obtain a typical mean crustal thickness of $\mu_{cr} \sim 45 \pm 20$ km before the overturn events. Several reasons combined may explain this: First, the generally lower temperature and reduced volcanic activity do not allow for the generation of a very thick crust on an inter-overturn time scale ($\sim\Delta t_{OT}$). This time scale is determined by the growth of crust itself. As soon as the crustal roots reach the stability field of denser eclogite (i.e., below 65 km in our model), the negative buoyancy of the dense root acts as a trigger to initiate the overturn event by causing excess stress. This implies that the interval between overturns depends on the density contrast of eclogite and the surrounding lithosphere for which we have not investigated different values here. But the timing will also depend on how much stress the lithosphere can support, which is in our model simply controlled by the yield stress (see Section 3.3.1).

Globally, the average crustal thickness is strongly impacted by the time passed since overturn cessation, but the minimum value is observed when the recycling is still ongoing (Figure 7). Here, mean crustal thickness never reaches very small values because of the finite duration of the event. Although effectively global in our model, crustal recycling in fact happens locally in typically only one major downwelling zone (Figure 6). It takes time to move all pre-overturn crustal material to the recycling zone and while this happens, volcanic activity is revived already in other parts and leads to the formation of new crust (Figure 7).

Typically, resurfacing events are considered to be global, that means they affect the entire lithosphere. Weller and Kiefer (2020) present another possible scenario, where an overturn initiates, but involves only part of the whole planetary surface and then ceases after resurfacing the thickest crustal roots that induce most of the lithospheric stress. In case E50_3e20, a globally young surface seems to indicate an overturn event with a global resurfacing (indicated in Figure 7f by the local surface ages that are all younger than the time passed since the onset of the overturn). However, the resulting crust after the overturn still features a small portion of surface with a thick crust that survived the overturn (Figure 7g). Comparing the distributions of mean surface age with crustal thickness reveals that for some cases this thick, preexisting crust features a very young (i.e., reset) surface, because a thin layer of fresh crust was emplaced on top. However, the existence of a substantial amount of young basalts on top of thick crustal provinces may not be entirely realistic. If isostatically compensated, a low crustal density would cause uplift and thus high topography. Lava may then flow down the topographic gradient, away from these regions, but our model is not yet capable of treating lateral lava flow. In addition, volcanic eruption efficiency may be reduced in regions with thick crust as it is more difficult for rising magma to overcome the integrated strength of the crust. An intrusive mode of magmatism would be more realistic here and will be investigated in future.

Our surface age diagnostic only considers the shallowest layer (uppermost cell) of our model and does not provide any information on how the crustal age changes with depth. We applied therefore model tracers to also track information about when the material was last molten to infer an alternative age, which considers only volcanic resurfacing, but not tectonic resurfacing (Noack, 2009). Both diagnostics seem to lead to almost identical results in stagnant-lid situations. For the episodic regime during overturn events, the measure without tectonic resurfacing typically predicts somewhat older age than expected, but the difference is rather small (not more than a few percent), which indicates that volcanism remains the main resurfacing mechanism even during overturn events.

The tracked property "age since last molten" is not limited to the surface layer, but available globally. Typically, the youngest ages are observed at the surface and just below the thermal boundary layer within the major zone of melting, below which age strongly increases toward the lower mantle. Within the crust and lithosphere, however, the age since last molten is larger than below and atop this zone. This demonstrates

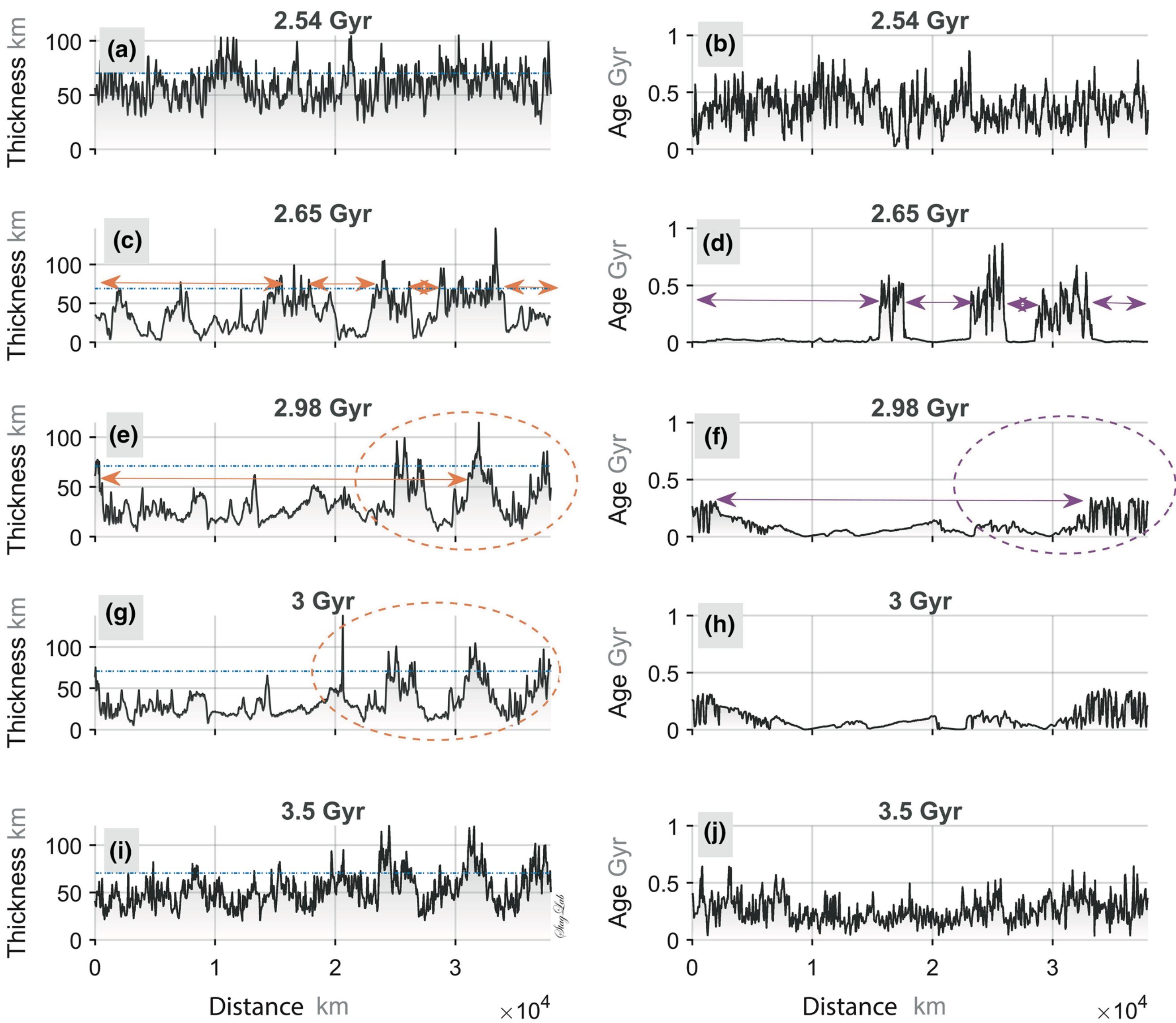

Figure 7. Lateral variation of (left) crustal thickness and (right) surface age during the overturn event shown in Figure 6. In the thickness panels, the horizontal dashed line denotes the transition depth to eclogite. The arrows span the area that underwent resurfacing since the onset of the overturn and the ellipses indicate a region with provinces of surviving older crust. Note that surface age can still be reset (=very low) in places with a thicker and older crustal province as the surface ages diagnostic only considers the shallowest layer: a thin layer of fresh crust on top of an older crustal root would still indicate a very low surface age.

that relatively old crustal material can persist in the shallow subsurface, but it is not directly apparent in our pure surface diagnostics, which does not capture the full effect of the recycling process.

3.3. Overturn Frequency and Intervals

The occurrence and timing of overturn events is highly dependent on the balance of the level of stress the lithosphere can support and the level of stress generated and induced into the lithosphere either by sub-lithospheric mantle flow or by surface loads, like negatively buoyant thick eclogitic roots. Effectively, this balance is here defined by the yield stress and the reference viscosity. Therefore, we investigate the impact of these control parameters on overturn frequency and intervals.

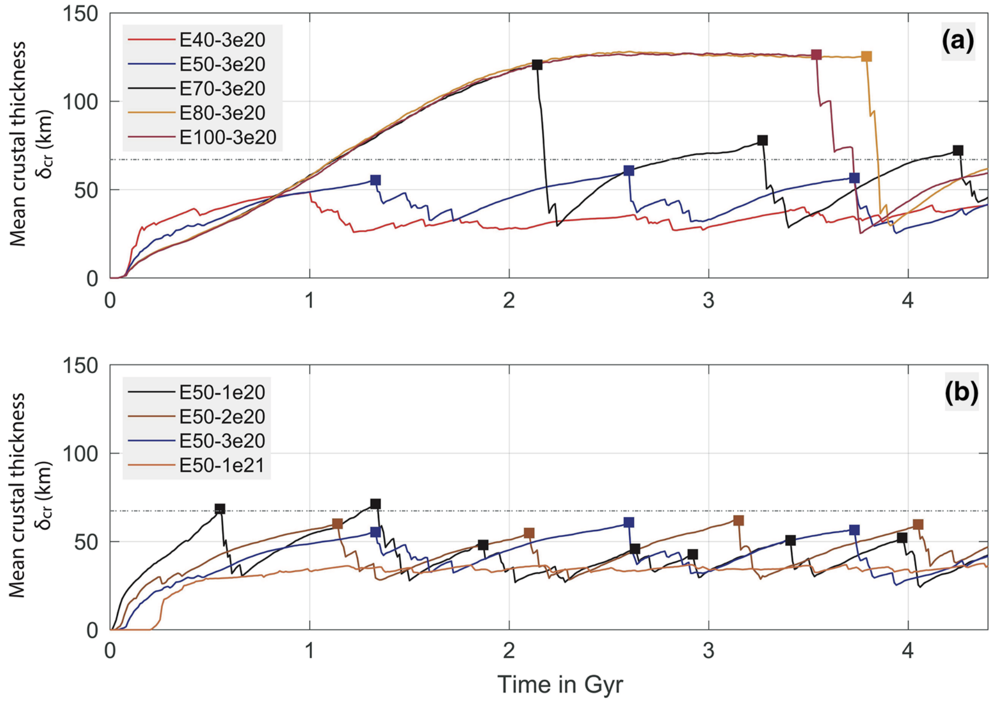

Figure 8. Mean crustal thickness in episodic cases with (a) variable yield stress and (b) variable reference viscosity. The square markers indicate the overturn initiation timing in the respective cases, which are distinctively spaced apart. The horizontal dashed-dotted line denotes the transition depth to eclogite.

3.3.1. Yield Stress

We investigate a range of surface yield stresses $\left(40 \leq \sigma_0 \leq 100 \quad \text{MPa}\right)$, while keeping the reference viscosity at $\eta_0 = 3 \times 10^{20}$ Pa s. We define overturn events by a combination of high surface mobility and abrupt crustal thickness variations. In comparison with the reference case (E50_3e20, $\sigma_0 = 50$ MPa), lower yield stress cases display more frequent overturns. The higher the yield stress, the later the first overturn event initiates (Figure 8a). This is clearly because the lithosphere can support more stress, while the convective stress generated stays approximately the same. More extensive eclogitic crustal roots are thus necessary to initiate the first overturn. In our highest yield stress cases, it takes more than 3.5 Gyr before an overturn occurs. Interestingly, for the cases with higher yield stress than in the reference case, mean crustal thickness reaches equilibrium much earlier (at ~2.5 Gyr), while there is no clear pattern for the first overturn to occur. This probably means that overturn events are triggered locally and not when the crust reaches an equilibrium average crustal thickness. The value of equilibrium average crustal thickness is not reached again after the first overturn event.

Overturn events at low yield stress occur with considerably shorter quiescence phases between them and start to resemble a mobile lid regime in which surface mobilization is continuous and no distinct events are present anymore. In intermediate cases $\left(50 \leq \sigma_0 \leq 70 \text{ MPa}\right)$ overturn events are somewhat regularly spaced although with different length of the quiescence phase. Our results do not allow discussion of this trend in the high yield stress cases, because these feature only a single overturn event within the entire integration time.

At high yield stress ($\sigma_0 \geq 80$ MPa) when the time until initiation of the first overturn is long, the crustal thickness evolution resembles that of the corresponding stagnant lid case with a large mean thickness of 120 ± 5 km just before overturn onset. With lower yield stress, overturns initiate early and crustal thickness cannot grow up to its equilibrium stagnant-lid thickness, but no clear trend between the crustal thickness

10.1029/2019JE006258

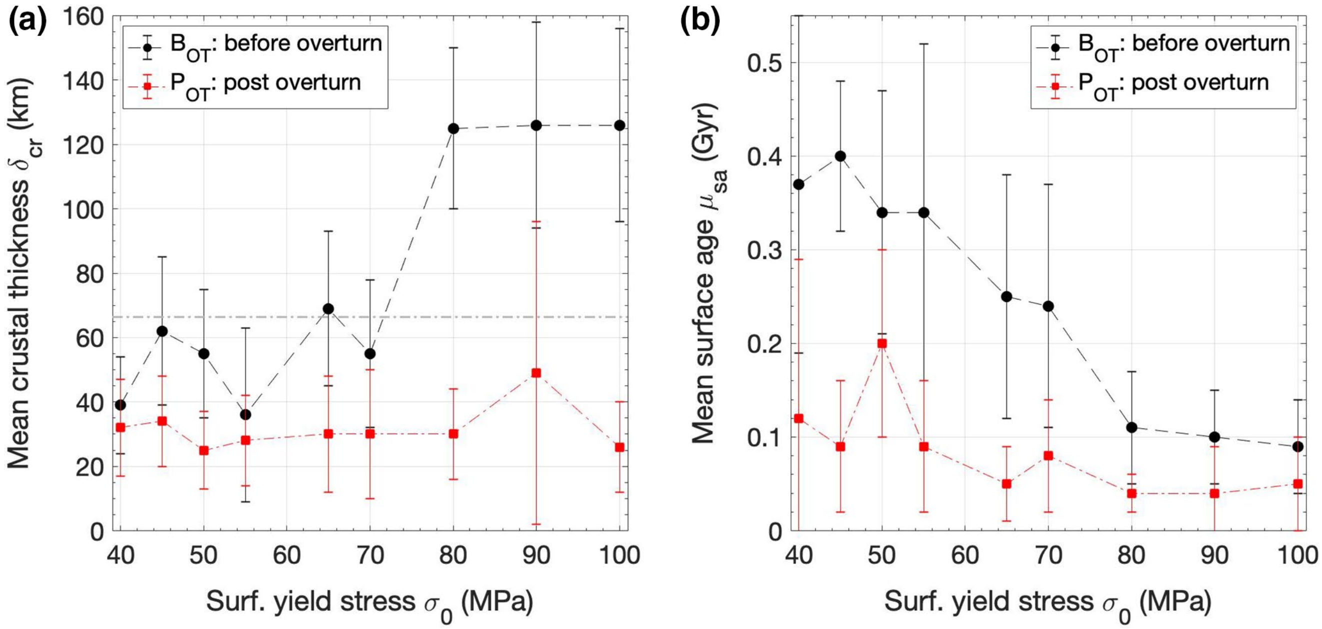

Figure 9. Effect of the yield stress on (a) mean crustal thickness and (b) surface age, both plotted for the time just before the onset of an overturn event (B_{OT}) and just after its cessation (P_{OT}). Error bars represent the corresponding $\pm 1\sigma$ standard deviation. The horizontal dash-dotted line in (a) indicates the transition depth into dense eclogite.

before the first overturn and the yield stress is visible (Figure 9a). For the range of yield stresses tested, the mean crustal thickness is reduced to a value of 25–35 km during the overturn event (case E90_3e20 with δ_{cr} ~50 km being a moderate exception, Table 4). While the actual numeric value should not be overinterpreted, this may approach the equilibrium crustal thickness expected for typical mobile lid scenarios. On the other hand, for the E50–E70 cases, the crustal thickness ranges between the values of 45–70 km just before the overturn, meaning that the resurfacing rate and thus crust production between the overturns (Δt_{OT}) is reduced to 30% of the rate during the overturn (Figure 9a). This in turn resembles the eruption rates for stagnant lid models. The duration of the overturn event seems to control the surface age, which is on the order of 80–400 Myr (Figure 9b). Thus, the process of rejuvenation of the crustal surface is for the high yield stress cases dominated by volcanic rather than tectonic resurfacing.

In addition, surface age is examined just before and just after overturn (Figure 9b). Before the overturn occurs, the surface is oldest with the weakest lithosphere and youngest with the strongest lithosphere (i.e., with the highest yield stress). This may appear counterintuitive initially, because a weak lithosphere allows for frequent surface mobilization and thus a more continuous recycling of lithosphere and crust. With a strong lithosphere and long inter-overturn interval, however, the sub-lithospheric mantle remains hotter, thus generates more melt and ultimately leads to a higher rate of volcanic resurfacing. After cessation of the overturn, mean surface age is generally very low and does not vary largely across the range of yield stress investigated here. Again, we emphasize that this diagnostic only considers the shallowest layer of our model.

3.3.2. Reference Viscosity

Changing the reference viscosity influences the level of stress τ generated in the model. On the other hand, stress is also proportional to strain rate $\dot{\varepsilon}$ (as $\tau \sim \eta \dot{\varepsilon}$), which is a function of flow velocity and in turn depends inversely on viscosity. In scaling laws, which typically invoke nondimensional parameters like the Rayleigh number (proportional to the inverse reference viscosity), convective stress increases with the Rayleigh number (e.g., Höink et al., 2012; Moresi & Solomatov, 1998), and thus decreases with reference viscosity. This implies a smaller feasibility of surface mobilization and overturn events with larger reference viscosity (smaller Rayleigh number) (e.g., Stein et al., 2013). However, if the scaling is converted back to dimensional viscosities, this trend reverses and convective stress is expected to decrease with decreasing reference viscosity (see van Heck, 2011). Comparing cases E50_1e21 and E50_3e20 (Table 4; Figure 8b) confirms this as the former case produces enough stress to continuously break the lithosphere (forming a quasi-mobile lid), while the latter case only produces a small number of distinct overturn episodes. For the other cases, this trend does not hold. Upon further reduction of the reference viscosity, the number of overturns increases again (e.g., $N_{\mathrm{OT}} = 7$ in case E50_1e20 compared to $N_{\mathrm{OT}} = 3$ in case E50_3e20).

In all of these cases, the frequency of overturns is too high to allow crustal thickness to reach its equilibrium thickness, as observed in the corresponding stagnant-lid models (Figure 8). An exception is model E50_1e21 without pronounced overturns, where the mean crustal thickness before overturn onset is 50–60 km. Crustal thickness after the overturn is between 25 and 35 km and does not seem to follow a trend. The relatively small drop in mean crustal thickness (compared to cases E80_3e20 or E_100_3e20 for instance) is an indication that individual overturn events are not as vigorous as they are in the higher yield stress regime close to the transition to a continuous stagnant lid.

In the evolution of mean surface age, the youngest surface before the overturn onset is seen with the lowest reference viscosity (200 Myr or less, Figure 10a), because this case features a high number of overturns and the highest rate of volcanic resurfacing. With our nominal reference viscosity ($\eta_0 = 3 \times 10^{20}$ Pa s), both of these aspects are reduced allowing for a pre-overturn surface age up to 400 Myr (Figure 10c). A similar level of surface age is observed with the highest reference viscosity ($\eta_0 = 1 \times 10^{21}$ Pa s, Figure 10d), but without the abrupt decrease in surface age typical for pronounced overturn events. In all tested cases, lateral age variations are quite strong (sometimes exceeding ±100% of the mean age) and the distribution thus seems not representative of a rather uniform planetary surface age.

3.4. Comparison to 3D Spherical Geometry

To test whether our model results are not strongly affected by the employed 2D spherical annulus geometry, we recomputed cases S2e20 and E50_2e20 in 3D spherical geometry. For computational feasibility, we had to use a reduced grid resolution of $64 \times 192 \times 64$ grid cells for each grid blocks of the Yin-Yang grid (Tackley, 2008). In stagnant lid, the predicted evolution of mean crustal thickness is very similar in 2D and 3D. The crustal growth rate seems somewhat smaller in 3D, so that the equilibrium thickness is reached later. After this point, however, mean crustal thickness differs only by ∼6% between 2D and 3D (see Figure S2). For surface age, however, the geometric differences are clearly more pronounced, because we observe a strong increase in surface age when changing from 2D to 3D. This is mostly explained by the different radial grid resolutions as the thickness of the "surface layer" within which tracer ages are averaged is tied to the numerical grid in our simple approach. This implies that a coarser surface layer (3D) leads to greater surface age than a thinner surface layer (2D). Recomputing the 2D case with the same radial grid resolution as in 3D leads to much more similar mean surface ages in 2D and 3D (see Figure S2). However, the apparent mesh sensitivity of our method should be improved in future work.

In the episodic regime, we observe very similar evolutions in mean crustal thickness for 2D and 3D. In both cases, four major overturn events are predicted within 4.4 Gyr of evolution, but the exact timing and duration of these events differ to some degree. A tendency that mean crustal thickness is larger just before the onset of the overturn event in 3D than in 2D is observed, but this has not been investigated in detail further. In 3D, we further observe that overturn events initiate locally and then spread and affect the surface globally (Figure 11), which is consistent with Rolf et al. (2018). Nevertheless, some provinces of old surface and/or thick crust are retained (Figures 11 and S4) and apparently survive recycling during the overturn event. While similar qualitative behavior is observed in 2D (case E50_2e20), the size and distribution of surviving patches is certainly affected by model geometry. Weller and Kiefer (2020) recently reported the survival of parts of the surface during overturn, but so far it remains unclear what controls the growth of overturn events from local to global overturns and under which conditions how much pre-overturn surface material can be maintained. Future 3D models using our framework aims to address these issues.

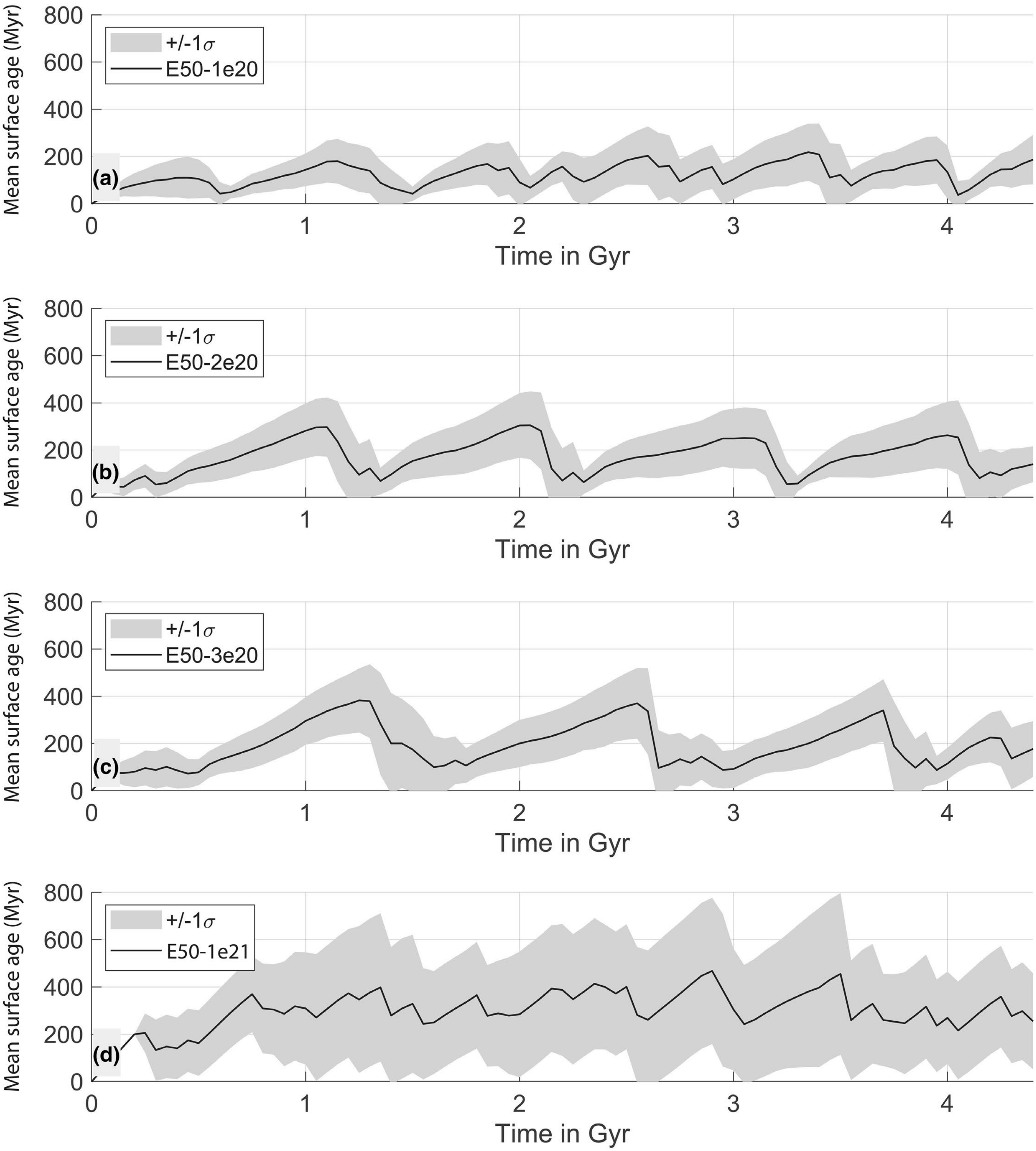

Figure 10. Time evolution of (a–d) mean surface ages of episodic models with variable reference viscosity as listed in Table 2. The shaded regions represent the corresponding $\pm 1\sigma$ standard deviation.

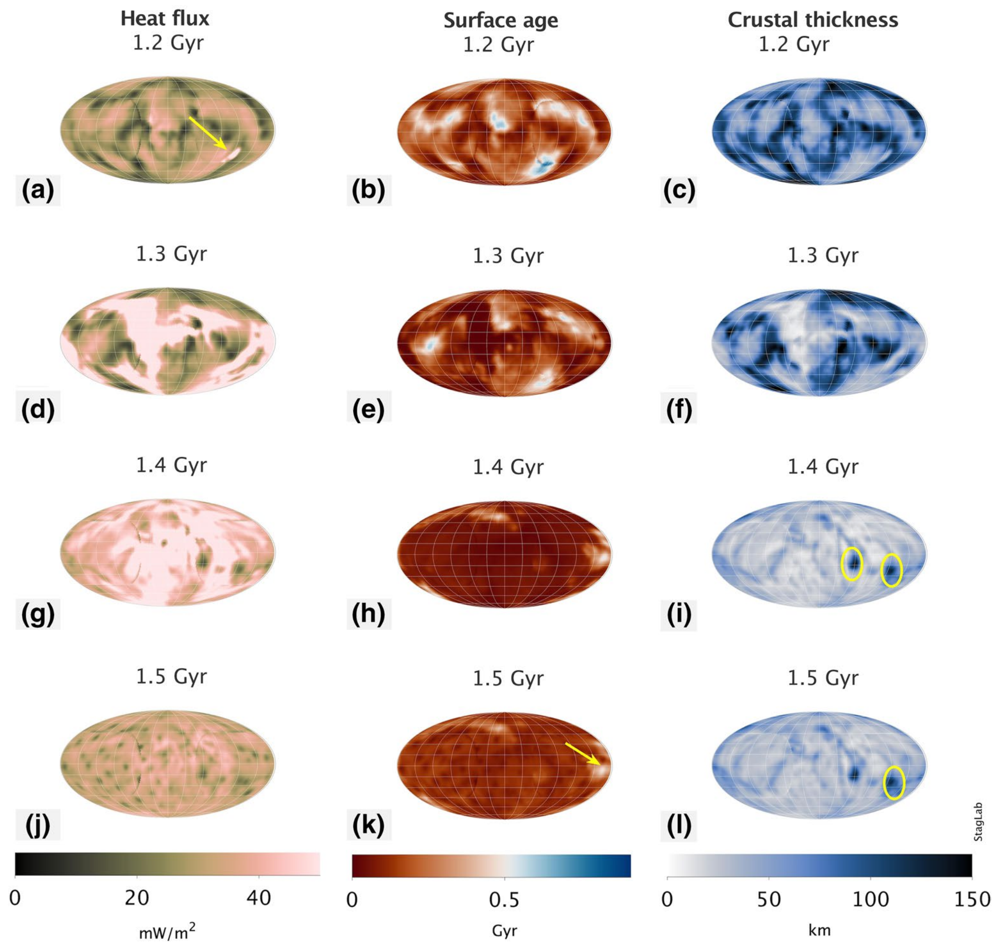

Figure 11. Mollweide projections of (left) heat flux, (middle) surface age, and (right) crustal thickness from the episodic case E50-2e20-3D. Shown are four different time steps that depict the evolution during an overturn event. Yellow arrows in the surface age maps indicate anomalously old surface; yellow ellipses in the crustal thickness maps indicate regions with anomalously great crustal thickness.

4. Discussion

In this study, we investigated parametric controls on the convective regime and the consequences for crustal thickness and surface age. In this section, we summarize the key findings and discuss their potential relevance for Venus and its resurfacing history.

4.1. Crustal Thickness Predictions

On Venus, we find several regions with high standing topography (*terrae* and *regiones*). These include crustal plateaus, which themselves comprise heavily deformed terrains (*tesserae*) and volcanic rises differing morphologically. Based on gravity data, the latter forms the thickest crustal provinces (e.g., comparable to Themis Regio) and are often observed above the major mantle plumes, which are rather stationary and source the volcanism above them (Stofan et al., 2016). The crustal plateaus have been suggested to resemble “pulsating continental crust,” crustal units that remain unrecycled, but experience phases of lateral compression and decompression (Romeo & Turcotte, 2008). Additionally, based on the correlation of topography and gravity, many rift-volcanic constructs are supported by dynamic topography (Steinberger et al., 2010). Our modeling attempts to reproduce such variations in crustal thickness (and comparable global mean values) and link them to the internal dynamics of the planet.

Direct measurements for crustal thickness on Venus (e.g., from seismic data) do not exist to date, but other methods allow for indirect estimates. Inversion of the observed gravity to topography ratios suggests a mean crustal thickness of less than 25 km, perhaps even less than 10 km (James et al., 2013). Wei et al. (2014) suggest a crustal thickness range of 30–70 km and Anderson and Smrekar (2006) a range of 0–90 km. All these values are below our predictions in the continuous stagnant lid, which suggest mean crustal thicknesses of 98–200 km. Previous studies using a similar model setup reached the same conclusion (Armann & Tackley, 2012; Jiménez-Díaz et al., 2015; Rolf et al., 2018).

However, we find that crustal thickness decreases with lower reference viscosity due to more dripping and convective erosion at the crustal base. Figure 5 suggests a thickness reduction by a factor of about 2 (from ~200 km to ~100 km), if the reference viscosity is reduced by factor 30. If this trend was to be extrapolated to lower viscosities, our models would match the above estimates with a reference viscosity in the range of 10^{17}–10^{19} Pa s only. This does not seem to align with the mantle viscosity profiles inferred for Venus from geoid inversion, which suggest upper mantle viscosity to be ~10^{20}–10^{21} Pa s (Benešová & Čížková, 2012; Rolf et al., 2018; Steinberger et al., 2010). Thus, reference viscosity alone does not seem to explain the different estimates. If heat-producing elements partition preferentially into the basaltic melt and are thus enriched in the surface crust, this would reduce mantle temperature and limit the amount of melting and crustal production subsequently. Armann and Tackley (2012) demonstrated that this effect helps to reduce the resulting crustal thickness, but not sufficiently, unless the partitioning would be much stronger than expected from typical Earth values.

A more likely reason is that magmatic activity and melt formation in the interior of a planet like Venus do not necessarily lead to volcanic eruption at the surface. Instead, intrusions may form in or at the base of the crust. For the Earth, more than 80% of magmatism may be intrusive (Cawood et al., 2013; Crisp, 1984), so the effect is substantial. For computational reasons, we could not consider partitioning into volcanic eruption and magmatic intrusions here, as this requires a distinct treatment of heat transport in melt pockets (e.g., Lourenço et al., 2018) that dramatically increases computation time. As an initial step into this direction (see Supporting Information S3), we tested some cases in which we simply reduced the eruption efficiency of the melt. This means only a portion of the melt is extracted and emplaced at the surface, but the rest is left behind in its original place and further transported by the evolving flow. Effectively, however, this merely leads to a slowdown in basalt extraction and a longer time is needed to reached equilibrium. Once obtained, mean crustal thickness does not seems to vary strongly with different eruption efficiencies (Figure S5). In terms of surface age, differences are more pronounced as this diagnostic is directly related to the rate of volcanic eruptions and thus to the eruption efficiency. In particular, low eruption efficiencies (<30%) promoted lateral age variations (Figure S6) as eruption of material is much reduced in regions above relatively cold upper mantle. These results indicate the importance of implementing a more realistic partitioning into volcanic eruption and magmatic intrusion into our model in future.

Considering magmatic intrusions would additionally imply that hot material penetrates the crust at shallow depths, which will weaken the strong surface layer and effectively allows for more crustal recycling and an effective thinning of the lithosphere (Lourenço et al., 2018). This may also affect the mobilization of the lithosphere since Lourenço et al. (2018) report a sluggish style of surface mobility with substantial intrusive volcanism even at yield stresses large enough to inhibit large-scale tectonic overturns. How intrusions may alter the timing, frequency, and vigor of overturn events has not been investigated and is an interesting prospect for future studies.

Overturn events generally help to limit the crustal thickness to levels of 20–65 km in our suite of cases. This range is more compatible with previous estimates (Jiménez-Díaz et al., 2015), because overturns recycle crustal layers and tectonically reset crustal thickness. In the episodic-lid regime, the actual crustal thickness depends strongly on the rate of eruptive volcanism and crustal growth, but also on the time that passed since overturn cessation. The shorter the time that passed since the last overturn, and the lower the eruption rate, the thinner is the crustal layer. This has motivated us to investigate the dynamics of lithospheric overturns, their conditions of occurrence, their duration, and frequency with our model.

Our episodic models suggest that both yield stress and reference viscosity significantly influence the overturn frequency and definitively impact the duration of the overturn events (Figure 8). The average crustal thickness can be considerably reduced with short overturn events lasting ~80–150 Myr. On a time scale comparable to Venus's entire history (~4.4 Gyr), the mean crustal thickness at the end of the model runs shows dependency largely on the time since the last overturn, the crust formation rate becomes considerably lower than during the overturn period. The time periods between subsequent overturn events are found to be considerably shorter with decreasing yield stress and are around 50–350 Myr.

During the cessation period, especially in cases where an overturn occurs early (at ~0.75–1 Gyr), some crustal regions are found to survive the overturn. This leads to a crust that is in certain regions as much as 20–40 km thicker than the surrounding crustal regions across the surface, and may resemble the plateau-like highlands (Grimm, 1994). These regions surviving at least the first overturn could be comparable to the prominent tessera regions on Venus, which are slightly more elevated than the vastly spread regional lava plains and may make about 10% of the surface (e.g., Hansen et al., 2000). However, the preservation of these surviving structures may be affected by the lithospheric rheology assumed here for which we have taken a fixed set of parameters that provided reasonable geodynamic behavior (e.g., the friction coefficient, activation energy, activation volume, and others). For future work, variation of these uncertain parameters is desirable to map out under which conditions how much pre-overturn surface material survives a major resurfacing event.

Either way, it is evident that resurfacing is highly nonuniform in all the episodic models. Nevertheless, our episodic models are more successful in reproducing the crustal thickness distributions of the order of the values applicable to the different geologic units on Venus.

4.2. Modeled Surface Age in Relation to Venus

In principle, the surface age derivation on Venus is an outcome of the planets' crater distribution. But the conversion of the observed crater frequencies is difficult to calibrate and to translate into an absolute age as this method has to make assumptions on the evolution of the impactor flux and on the detectability of crater structures, which may be modified by subsequent surface processes after the formation of a crater. Consequently, Venus's absolute surface age has significant uncertainty and a variety of mean ages between 150 and 1,000 Ma have been suggested (Hauck et al., 1998; McKinnon et al., 1997; Nimmo & McKenzie, 1998; Strom et al., 1994), with an often used nominal value of 750^{+350}_{-400} Myr (McKinnon et al., 1997).

In our suite of stagnant-lid models, the surface always remains very young, typically 100–150 Myr (Table 3). Only with very high reference viscosity (case S1e22) the surface was slightly older than 250 Myr or if melt eruption efficiency is very low (supplementary case S3e20_20%), because in these cases the rate of volcanic resurfacing is low enough to allow the surface to grow older. Further increasing the reference viscosity does not match Venus's viscosity profile inferred from geoid inversion and is thus an infeasible approach. Some further reduction of the melt eruption efficiency may be feasible as terrestrial ratios of extrusive to intrusive volumes of volcanism may be as low as ~10% (Crisp, 1984). With such low eruption efficiencies, it seems likely that the observationally inferred mean age of Venus's surface could be matched with our stagnant-lid models, especially if the possibility of forming intrusions is considered (Lourenço et al., 2018). We also emphasize that surface age estimates based on crater statistics have a substantial spread. Herrick and Rumpf (2011), for instance, argued that the volcanic and tectonic postimpact modification apparent for many Venusian craters may require a reduced surface age of ~150 Myr. In such a case, our stagnant lid model predictions (Figure 5b) would fit the observational estimate even with purely extrusive volcanism, although this remains an unlikely end-member for a planet like Venus.

It should be emphasized again that our estimate of absolute surface age depends on the radial grid resolution at the top of the model domain (here ~20 km). Averaging age over all tracers in a thicker (thinner) surface layer should lead to older (younger) absolute surface age. An additional simplification of our estimate is that we neglect lava flows down topographic gradients that potentially cover large areas. These caveats that should be addressed in future models may lead to systematic offsets in our absolute age estimates, however, a comparison between our models is still useful.

Independent of the absolute mean age, it remains problematic in our stagnant-lid models to predict surface ages that do not vary strongly across the surface: the model-predicted standard deviation is at least 70% of the mean age (Table 3). In stagnant lid cases, the regions above hot mantle plumes are constantly resurfaced, while the regions away from these hotspots are much less resurfaced (and possibly by more than an order of magnitude older, see Figure 3). This contradicts the idea of a homogeneously young surface age for Venus. However, this trend is likely fostered by our assumption of 100% melt eruption efficiency. Independent of that and in the absence of properly calibrated (absolute) surface ages based on cratering statistics, refined mapping of Venus's geology has revealed a statistically significant spread in superposed craters (density) and thus in the age of Venus's surface features. Tesserae may be substantially older (1.47 ± 0.46-times the mean age (Ivanov & Basilevsky, 1993), so they could predate an catastrophic overturn episode (Hansen & López, 2010). On the other end of the spectrum, the age of the youngest volcanic features reach only ~40% of the mean age (Kreslavsky et al., 2015; Price & Suppe, 1994). This is consistent with the growing body of evidence for ongoing or at least very recent volcanism (e.g., Filiberto et al., 2020; Gülcher et al., 2020; Smrekar et al., 2010; Stofan et al., 2016). However, such extreme features may concern only relatively small portions of the surface; the tesserae only cover 10% of the surface after all. Consequently, such strong variations as we observe in most of our stagnant lid cases seem little compatible with the geological mapping and crater statistics for Venus. In other words, our model fails to generate the characteristics of Venus's surface age under equilibrium resurfacing in a stagnant-lid scenario.

Our models with episodic overturns generally predict greater absolute surface age than the stagnant-lid models except during an ongoing overturn event or shortly after its cessation. Just before resurfacing begins, mean surface ages as old as 400 Myr can be observed even with 100% melt eruption efficiencies. Even larger surface ages can be expected in episodic models with lower eruption efficiencies. In tests with lower eruption efficiency, we observed that only 2% of the surface remain older than 500 Myr with 100% eruption efficiency due to a large average resurfacing rate of 3–5 $km^2\ yr^{-1}$, but with only 25% melt eruption efficiency already 12% of the surface become older than 500 Myr.

A sufficiently long time after overturn cessation, the overturn scenario seems better capable of reproducing absolute mean surface ages comparable to those suggested for Venus, while keeping in mind the potential offsets in our approach described above. This is because the mantle is globally cooler in this scenario and the rate of melting and volcanic resurfacing is reduced. Although the lateral variation of surface age with respect to the mean value is slightly lower than in the stagnant-lid suite (see Table 4), the problem with the uniformity of surface age persists also in this scenario, which still predicts strong lateral variations (Figure 10). While mean age grows during a long stagnant-lid phase between two overturns, the regions above the mantle plumes are still frequently resurfaced, while the other regions are less so, which causes strong lateral variation.

Conceptually, a close-to-uniform surface age can only be expected if resurfacing rates are similar across the entire surface. One extreme scenario to realize this would be a hot upper mantle without strong lateral temperature variation or, in other words, the absence of very hot plume heads in Venus's upper mantle. The absence of dynamo activity on Venus may be linked to rather low heat flow from the core into the mantle and consequently weak plumes, which could support this hypothesis. On the other hand, measurements made on Venus Express do suggest the presence of isolated regions with anomalously high thermal emissivity, which could be a surface signature of mantle plumes (Smrekar et al., 2010). Our models feature relatively strong heat flux across the CMB (Figure 1c); although we employ the same initial temperature of the CMB as in Rolf et al. (2018), our predictions of CMB heat flux is a factor of ~3–4 higher. The reason for this discrepancy is that we do not include the temporal adjustment of the CMB temperature throughout the evolution, which resulted in a significant decrease in bottom temperature and thus heat flux in that previous study. It is thus possible that our models overemphasize the strength of plumes and thus their role in shaping the distribution of volcanism. We note, however, that even with much weaker plumes, Rolf et al. (2018) were not successful in predicting surface age distributions without strong lateral variations; similar results were obtained in the study of Noack et al. (2012).

Another possible scenario to generate a very uniform surface age would be that volcanic resurfacing essentially vanishes at some point, because then the surface age would grow globally and uniformly after cessation of an overturn and can only be reset via a subsequent event of tectonic mobilization and resurfacing. If parts of the surface resist recycling by the terminal overturn, this would still lead to old, but less uniform surface ages, which possibly explains the observational record best. However, several studies suggest dormant volcanic activity on Venus (Bondarenko et al., 2010; Shalygin et al., 2015; Smrekar et al., 2010), which rejuvenates the surface and works against this possibility, unless the volumes of recent volcanism are sufficiently small and limited to minor regions that do not distort the global mean. More in-depth analysis and comparison on both ends, numerical modeling and geological mapping, is thus necessary to understand Venus's resurfacing history. Currently, we cannot speculate any further whether and when volcanic activity could have diminished to a level where it does not affect the global mean surface age substantially anymore. This would (at least) require including long-term cooling trends related to the heat loss of the core and to the decay of heat-producing elements as well as their heterogeneous distribution in the mantle and lithosphere. Some additional complexities, such as those listed in Section 4.4, could additionally help to resolve which particular geodynamic evolution can generate a rather uniform surface age.

4.3. Overturn Frequency Dependence on Viscosity

We studied how the choice of reference viscosity influences the level of stress generated in the model, which is generally expected to depend on both viscosity and strain rate. The latter is itself a function of flow rate and (inversely) of viscosity. Scaling arguments from boundary layer theory for plane-layer, isochemical convection (Höink et al., 2011, 2012) suggest that convective stress shall decrease with decreasing mantle (reference) viscosity (van Heck, 2011). This would imply a tendency to less plastic yielding in the lithosphere and thus less overturns and surface mobilization. But our modeling results with changing reference viscosity do not confirm this in a simple manner as the model behavior is nonlinear and the tendency for overturns to occur first decreases and then increases again by reducing the reference viscosity.

An explanation for more frequent overturns with lower reference viscosity could be given by the fact that the yield stress increases with depth and what matters for overturn initiation is not only its surface value but also the level at the base of the lithosphere, because the entire lithosphere needs to undergo yielding to develop subduction-like behavior (Crameri & Tackley, 2016; Höink et al., 2011, 2012). With a constant friction coefficient in all cases, this base value is determined by lithospheric thickness, which is known to decrease with reference viscosity. Effectively, the integrated strength of the lithosphere is then lower and it may thus yield at a somewhat smaller level of convective stress. Such scaling relations have been investigated previously (e.g., Moresi & Solomatov, 1998), but in simpler systems without melting and volcanism. The loading of the lithosphere with basal crust (and eventually eclogitic roots) changes the stress in the lithosphere and the boundary layer thickness as a function of reference viscosity. Further details are beyond the scope of this paper, but these aspects could explain the nonlinear trends in overturn frequency observed in our models with varying reference viscosity.

Internal heating (as a parameter) also influences these relationships. For example, Weller et al. (2015) studied the impact of internal heating on the transition of tectonic regimes on large timescales and highlighted the strong sensitivity to yield strength. Similarly, Stein et al. (2013) argue that the tendency of surface mobilization decreases with increasing internal heating rate. Our results closely agree with their results: although we keep the internal heating rate constant throughout the presented models, we tested both higher and lower internal heating rates compared to the nominal value used here. As internal heating rates decrease with time during planetary evolution, higher (lower) internal heating rates may reflect earlier (later) stages of Venus's history, although this simple comparison must be taken with care. Higher internal heating would be expected to cause a hotter and less viscous mantle and thus less stress induced to the lithosphere. The thinner thermal boundary layer may allow for more magmatic activity, so that thicker crust and a younger surface are expected in the stagnant lid regime of evolution. However, if the crust grows too thick in places, its base transforms to dense eclogite and results in larger stresses in the crust and lithosphere. This modulates the initiation of overturns (Section 3.3) and it is not clear what the net result on the tectonic evolution would be.

4.4. Model Limitations

The models presented for Venus's thermochemical mantle evolution are based on the earlier study of Rolf et al. (2018) and thus inherit similar assumptions taken in their work. This includes mantle incompressibility and neglecting the coupling to the atmospheric evolution (e.g., Gillmann & Tackley, 2014; Gillmann et al., 2016) as well as any previously existing water and volatile recycling. The initial conditions for Venus are only speculative at best and assumed ad hoc in our model. Moreover, the influence of many parameters and properties of the model still remain uncertain. These initial assumptions certainly have some effect on the dynamic evolution presented in our models and should therefore be tested further in the future.

For the main focus of this work, however, the simplifications made on the melting and magmatism description are probably most notable, as already discussed in the previous sections. Another important limitation is that our model has a 2D geometry. In a 3D model, overturn and mantle plumes could evolve somewhat differently. As the regions above plumes are the hottest and prone to the most efficient volcanic resurfacing, changing to 3D geometry could have important effects on the predicted age distribution since plumes are 3D features. While we presented two example cases in 3D, a larger set of 3D models would allow to compare our model more directly to correlations with specific geological features on Venus. Furthermore, implementing the combination of various styles of magmatism in 3D modeling environments can refine the models presented here. Indeed, considering intrusive magmatism rather than modulating the eruption efficiency, as in Lourenço et al. (2018), is an essential next step to understand Venus's cooling and the resulting surface age distribution better.

Despite such model limitations, our models capture key aspects of the dynamically evolving planetary mantle of Venus and can, under considerations of their limits, yield important insights into how a system so similar to Earth in size and composition, evolve so differently over geologic time scales.

5. Conclusions

We carried out a systematic parametric study of Venus's interior dynamic evolution, considering both a potential stagnant (corresponding to equilibrium resurfacing) and a potential episodic lid regime (corresponding to catastrophic resurfacing) with the goal to refine which regime works better to explain Venus's surface characteristics. In stagnant lid, our models predict thicker crust and result in a much younger surface than commonly inferred for Venus. This suggests a too high rate of volcanic resurfacing in our models. Reducing the efficiency of melt eruption and thus of volcanic resurfacing may help reducing this rate, especially if melt eruption efficiency is <30%, but then the resulting age distributions feature very strong variations between regions atop main mantle plumes and those regions atop colder mantle. Future implementation of partitioning into extrusive volcanism and intrusive magmatism seems necessary.

In the episodic lid regime, the timing and interval of overturn events is highly dependent on the lithospheric yield stress. With a yield stress close to the threshold value of the stagnant-lid regime, only one, or very few, clearly distinct overturn episodes occur, while lower yield stress allows for more frequent overturns, which at some point begin to resemble a continuous mobile lid regime. With overturn episodes, crustal thickness is generally reduced, and, even after a long period of tectonic quiescence, the large equilibrium value of the stagnant-lid regime is not reached. Overturns generally reduce mantle temperature due to recycling of cold material into the interior and thereby reduce the rate of volcanic resurfacing during the inter-overturn phases of the model evolutions. This can lead to an older surface on average (up to 400 Myr). After cessation of an overturn event, the entity of the surface seems to be renewed, so that the surface on average appears very young. However, this surface appears young because of a very thin layer in places underlain by thick old crustal roots that originate from the pre-overturn period. Such a thin surface layer modified by subsequent crustal process could still disguise the underlying old roots and represent anomalously thick but actually old features in the surface age distributions such as, perhaps, tesserae on Venus.

Both resurfacing regimes generally suggest substantial spatial variations, in crustal thickness but also in surface age, because the regions atop hot mantle plumes feature faster crustal growth and thus a younger surface than those regions overlying relatively colder mantle, especially in episodic models. A higher degree of uniformity in predicted surface age may be achieved by further reducing the rate of volcanism, for instance via more efficient mantle cooling in general, or by a smaller fraction of eruptive to intrusive volcanism, or probably by a combination of both. Overall, our modeling still suggests that a regime with large-scale tectonic overturns, that mobilize the entire surface but do not necessarily recycle the whole entirety of surface material, is more promising than a pure stagnant-lid regime of equilibrium resurfacing, but Venus's true dynamic regime cannot simply be expressed by either option.

Data Availability Statement

All data supporting our conclusions in this study can be obtained from an online data repository (Uppalapati, 2020).

Acknowledgments
We thank the I. Romeo, S. King, and L. Montesi (editor) for thoughtful comments that helped to improve the manuscript. Funding has been received from the Norwegian Research Council through a Centre of Excellence grant to the Centre for Earth Evolution and Dynamics (CEED, 223272). This work was partly supported by the Research Council of Norway through the funding to The Norwegian Research School on Dynamics and Evolution of Earth and Planets, project number 249040/F60. T. Rolf further acknowledges funding from the Norwegian Research Council through a Young Talents grant (PLATONICS, 276032). Computations were performed on Stallo, a Notur facility at University of Tromsø (project code: nn9010/ns9010). We thank P. J. Tackley for providing the code StagYY.

References

Abe, Y. (1995). Basic equations for the evolution of partially molten mantle and core. In T. Yukutake (Ed.), *The Earth's central part: Its structure and dynamics* (pp. 215–230). Tokyo, Japan: Terrapub.

Anderson, F. S., & Smrekar, S. E. (2006). Global mapping of crustal and lithospheric thickness on Venus. *Journal of Geophysical Research*, *111*(E8). https://doi.org/10.1029/2004je002395

Armann, M., & Tackley, P. J. (2012). Simulating the thermochemical magmatic and tectonic evolution of Venus's mantle and lithosphere: Two-dimensional models. *Journal of Geophysical Research*, *117*(E12). https://doi.org/10.1029/2012je004231

Benešová, N., & Čížková, H. (2012). Geoid and topography of Venus in various thermal convection models. *Studia Geophysica et Geodaetica*, *56*(2), 621–639. https://doi.org/10.1007/s11200-011-0251-7

Bindschadler, D. L., Schubert, G., & Kaula, W. M. (1992). Coldspots and hotspots' global tectonics and mantle dynamics of Venus. *Journal of Geophysical Research*, *97*(E8), 13495–413532.

Bjonnes, E. E., Hansen, V. L., James, B., & Swenson, J. B. (2012). Equilibrium resurfacing of Venus: Results from new Monte Carlo modeling and implications for Venus surface histories. *Icarus*, *217*(2), 451–461. https://doi.org/10.1016/j.icarus.2011.03.033

Bondarenko, N. V., Head, J. W., & Ivanov, M. A. (2010). Present-day volcanism on Venus: Evidence from microwave radiometry. *Geophysical Research Letters*, *37*(23). https://doi.org/10.1029/2010gl045233

Cawood, P. A., Hawkesworth, C. J., & Dhuime, B. (2013). The continental record and the generation of continental crust. *Geological Society of America Bulletin*, *125*(1–2), 14–32. https://doi.org/10.1130/b30722.1

Christensen, U. R., & Yuen, D. A. (1985). Layered convection induced by phase transitions. *Journal of Geophysical Research*, *90*(B12), 10291–10300. https://doi.org/10.1029/JB090iB12p10291

Crameri, F. (2017). *StagLab: Geodynamic diagnostics and scientific visualisation*. Retrieved from https://doi.org/10.5281/zenodo.1199037

Crameri, F. (2018). Geodynamic diagnostics, scientific visualisation and StagLab 3.0. *Geoscientific Model Development*, *11*(6), 2541–2562. https://doi.org/10.5194/gmd-11-2541-2018

Crameri, F., Conrad, C. P., Montési, L., & Lithgow-Bertelloni, C. R. (2019). The dynamic life of an oceanic plate. *Tectonophysics*, *760*, 107–135. https://doi.org/10.1016/j.tecto.2018.03.016

Crameri, F., & Tackley, P. J. (2016). Subduction initiation from a stagnant lid and global overturn: New insights from numerical models with a free surface. *Progress in Earth and Planetary Science*, *3*(1), 1–19. https://doi.org/10.1186/s40645-016-0103-8

Crisp, J. A. (1984). Rates of magma emplacement and volcanic output. *Journal of Volcanology and Geothermal Research*, *20*, 171–211.

Davaille, A., Smrekar, S. E., & Tomlinson, S. (2017). Experimental and observational evidence for plume-induced subduction on Venus. *Nature Geoscience*, *10*(5), 349–355. https://doi.org/10.1038/ngeo2928

Dumoulin, C., Tobie, G., Verhoeven, O., Rosenblatt, P., & Rambaux, N. (2017). Tidal constraints on the interior of Venus. *Journal of Geophysical Research: Planets*, *122*(6), 1338–1352. https://doi.org/10.1002/2016je005249

Filiberto J., Trang D., Treiman A. H., Gilmore M. S. (2020). Present-day volcanism on Venus as evidenced from weathering rates of olivine. *Science Advances*, *6*, (1), eaax7445https://doi.org/10.1126/sciadv.aax7445.

Frank, S. L., & Head, J. W. (1990). Ridge belts on Venus: Morphology and origin. *Earth and Planetary Science Letters*, *50/51*, 421–470.

Gillmann, C., Golabek, G. J., & Tackley, P. J. (2016). Effect of a single large impact on the coupled atmosphere-interior evolution of Venus. *Icarus*, *268*, 295–312. https://doi.org/10.1016/j.icarus.2015.12.024

Gillmann, C., & Tackley, P. (2014). Atmosphere/mantle coupling and feedbacks on Venus. *Journal of Geophysical Research: Planets*, *119*(6), 1189–1217. https://doi.org/10.1002/2013je004505

Grimm, R. E. (1994). The deep structure of Venusian plateau highlands. *Icarus*, *112*, 89–103.

Gülcher, A. J. P., Gerya, T. V., Montési, L. G. J., & Munch, J. (2020). Corona structures driven by plume–lithosphere interactions and evidence for ongoing plume activity on Venus. *Nature Geoscience*, *13*(8), 547–554. https://doi.org/10.1038/s41561-020-0606-1

Hansen, V. L., & López, I. (2010). Venus records a rich early history. *Geology*, *38*(4), 311–314. https://doi.org/10.1130/g30587.1

Hansen, V. L., & Phillips, R. J. (1995). Formation of Ishtar Terra, Venus: Surface and gravity constraints. *Geology*, *23*, 292–296.

Hansen, V. L., Phillips, R. J., Willis, J. J., & Ghent, R. R. (2000). Structures in tessera terrain, Venus: Issues and answers. *Journal of Geophysical Research*, *105*(E2), 4135–4152. https://doi.org/10.1029/1999je001137

Hauck, S. A., Phillips, R. J., & Price, M. H. (1998). Venus: Crater distribution and plains resurfacing models. *Journal of Geophysical Research*, *103*(E6), 13635–13642. https://doi.org/10.1029/98je00400

Hernlund, J. W., & Tackley, P. J. (2008). Modeling mantle convection in the spherical annulus. *Physics of the Earth and Planetary Interiors*, *171*(1–4), 48–54. https://doi.org/10.1016/j.pepi.2008.07.037

Herrick, R. R., & Rumpf, M. E. (2011). Postimpact modification by volcanic or tectonic processes as the rule, not the exception, for Venusian craters. *Journal of Geophysical Research*, *116*(E2). https://doi.org/10.1029/2010je003722

Höink, T., Jellinek, A. M., & Lenardic, A. (2011). Viscous coupling at the lithosphere-asthenosphere boundary. *Geochemistry, Geophysics, Geosystems*, *12*(10). https://doi.org/10.1029/2011gc003698

Höink, T., Lenardic, A., & Richards, M. (2012). Depth-dependent viscosity and mantle stress amplification: Implications for the role of the asthenosphere in maintaining plate tectonics. *Geophysical Journal International*, *191*(1), 30–41. https://doi.org/10.1111/j.1365-246X.2012.05621.x

Ivanov, M. A., & Basilevsky, A. T. (1993). Density and morphology of impact craters on tessera terrain. *Geophysical Research Letters*, *20*(23), 2579–2582.

Ivanov, M. A., & Head, J. W. (2011). Global geological map of Venus. *Planetary and Space Science*, *59*(13), 1559–1600. https://doi.org/10.1016/j.pss.2011.07.008
Ivanov, M. A., & Head, J. W. (2013). The history of volcanism on Venus. *Planetary and Space Science*, *84*, 66–92. https://doi.org/10.1016/j.pss.2013.04.018
James, P. B., Zuber, M. T., & Phillips, R. J. (2013). Crustal thickness and support of topography on Venus. *Journal of Geophysical Research: Planets*, *118*(4), 859–875. https://doi.org/10.1029/2012je004237
Jiménez-Díaz, A., Ruiz, J., Kirby, J. F., Romeo, I., Tejero, R., & Capote, R. (2015). Lithospheric structure of Venus from gravity and topography. *Icarus*, *260*, 215–231. https://doi.org/10.1016/j.icarus.2015.07.020
Keller, T., & Tackley, P. J. (2009). Towards self-consistent modeling of the martian dichotomy: The influence of one-ridge convection on crustal thickness distribution. *Icarus*, *202*, 429–443. https://doi.org/10.1016/j.pepi.2008.08.005
King, S. D. (2018). Venus resurfacing constrained by geoid and topography. *Journal of Geophysical Research: Planets*, *123*(5), 1041–1060. https://doi.org/10.1002/2017je005475
Kreslavsky, M. A., Ivanov, M. A., & Head, J. W. (2015). The resurfacing history of Venus: Constraints from buffered crater densities. *Icarus*, *250*, 438–450. https://doi.org/10.1016/j.icarus.2014.12.024
Le Feuvre, M., & Wieczorek, M. A. (2011). Nonuniform cratering of the Moon and a revised crater chronology of the inner Solar System. *Icarus*, *214*(1), 1–20. https://doi.org/10.1016/j.icarus.2011.03.010
Lenardic, A., Kaula, W. M., & Bindschadler, D. L. (1993). A mechanism for crustal recycling on Venus. *Journal of Geophysical Research*, *98*(E10), 18697–618705.
Lourenço, D. L., Rozel, A. B., Gerya, T., & Tackley, P. J. (2018). Efficient cooling of rocky planets by intrusive magmatism. *Nature Geoscience*, *11*(5), 322–327. https://doi.org/10.1038/s41561-018-0094-8
Lourenço, D. L., Rozel, A., & Tackley, P. J. (2016). Melting-induced crustal production helps plate tectonics on Earth-like planets. *Earth and Planetary Science Letters*, *439*, 18–28. https://doi.org/10.1016/j.epsl.2016.01.024
McKinnon, W. B., Zahnle, K., Ivanov, B. A., & Melosh, H. J. (1997). Cratering on Venus: Modeling and observations. In W. Bougher, D. M. Hunten, & R. J. Phillips (Eds.), *Venus II* (pp. 969–1014). Tucson, AZ: University of Arizona Press.
Moresi, L., & Solomatov, V. (1998). Mantle convection with a brittle lithosphere: Thoughts on the global tectonic styles of the Earth and Venus. *Geophysical Journal International*, *133*(3), 669–682. https://doi.org/10.1046/j.1365-246X.1998.00521.x
Nakagawa, T., Tackley, P. J., Deschamps, F., & Connolly, J. A. D. (2009). Incorporating self-consistently calculated mineral physics into thermochemical mantle convection simulations in a 3-D spherical shell and its influence on seismic anomalies in Earth's mantle. *Geochemistry, Geophysics, Geosystems*, *10*(3). https://doi.org/10.1029/2008gc002280
Nakagawa, T., Tackley, P. J., Deschamps, F., & Connolly, J. A. D. (2010). The influence of MORB and harzburgite composition on thermo-chemical mantle convection in a 3-D spherical shell with self-consistently calculated mineral physics. *Earth and Planetary Science Letters*, *296*(3–4), 403–412. https://doi.org/10.1016/j.epsl.2010.05.026
Nimmo, F., & McKenzie, D. (1998). Volcanism and tectonics on Venus. *Annual Review of Earth and Planetary Science Letters*, *26*, 23–51.
Noack, L. (2009). CIDGA: Coupling of interior dynamic models with global atmosphere models. In Science and Supercomputing in Europe (HPC-Europa2 Report 37).
Noack, L., Breuer, D., & Spohn, T. (2012). Coupling the atmosphere with interior dynamics: Implications for the resurfacing of Venus. *Icarus*, *217*(2), 484–498. https://doi.org/10.1016/j.icarus.2011.08.026
O'Rourke, J. G., Wolf, A. S., & Ehlmann, B. L. (2014). Venus: Interpreting the spatial distribution of volcanically modified craters. *Geophysical Research Letters*, *41*(23), 8252–8260. https://doi.org/10.1002/2014gl062121
O'Neill, C., Lenardic, A., Weller, M., Moresi, L., Quenette, S., & Zhang, S. (2016). A window for plate tectonics in terrestrial planet evolution? *Physics of the Earth and Planetary Interiors*, *255*, 80–92. https://doi.org/10.1016/j.pepi.2016.04.002
Papuc, A. M., & Davies, G. F. (2012). Transient mantle layering and the episodic behaviour of Venus due to the 'basalt barrier' mechanism. *Icarus*, *217*(2), 499–509. https://doi.org/10.1016/j.icarus.2011.09.024
Price, M. H., & Suppe, J. (1994). Mean age of rifting and volcanism on Venus deduced from impact crater densities. *Nature*, *372*, 22–29.
Reese, C. C., Solomatov, V. S., & Orth, C. P. (2007). Mechanisms for cessation of magmatic resurfacing on Venus. *Journal of Geophysical Research*, *112*(E4). https://doi.org/10.1029/2006je002782
Rolf, T., Steinberger, B., Sruthi, U., & Werner, S. C. (2018). Inferences on the mantle viscosity structure and the post-overturn evolutionary state of Venus. *Icarus*, *313*, 107–123. https://doi.org/10.1016/j.icarus.2018.05.014
Romeo, I. (2013). Monte Carlo models of the interaction between impact cratering and volcanic resurfacing on Venus: The effect of the Beta-Atla-Themis anomaly. *Planetary and Space Science*, *87*, 157–172. https://doi.org/10.1016/j.pss.2013.07.010
Romeo, I., & Turcotte, D. L. (2008). Pulsating continents on Venus: An explanation for crustal plateaus and tessera terrains. *Earth and Planetary Science Letters*, *276*(1–2), 85–97. https://doi.org/10.1016/j.epsl.2008.09.009
Romeo, I., & Turcotte, D. L. (2010). Resurfacing on Venus. *Planetary and Space Science*, *58*(10), 1374–1380. https://doi.org/10.1016/j.pss.2010.05.022
Rozel, A. B., Golabek, G. J., Jain, C., Tackley, P. J., & Gerya, T. (2017). Continental crust formation on early Earth controlled by intrusive magmatism. *Nature*, *545*(7654), 332–335. https://doi.org/10.1038/nature22042
Sandwell, D. T., & Schubert, G. (1992). Evidence for retrograde lithospheric subduction on Venus. *Science*, *257*(5071), 766–770.
Schaber, G. G., Strom, R. G., Moore, H. J., Soderblom, L. A., Kirk, R. L., Chadwick, D., et al. (1992). Geology and distribution of impact craters on Venus: What are they telling us? *Journal of Geophysical Research*, *97*(E8), 13257–13301.
Shalygin, E. V., Markiewicz, W. J., Basilevsky, A. T., Titov, D. V., Ignatiev, N. I., & Head, J. W. (2015). Active volcanism on Venus in the Ganiki Chasma rift zone. *Geophysical Research Letters*, *42*(12), 4762–4769. https://doi.org/10.1002/2015gl064088
Smrekar S. E., Stofan E. R., Mueller N., Treiman A., Elkins-Tanton L., Helbert J., et al. (2010). Recent Hotspot Volcanism on Venus from VIRTIS Emissivity Data. *Science*, *328*, (5978), 605–608. http://dx.doi.org/10.1126/science.1186785
Steinberger, B., Werner, S. C., & Torsvik, T. H. (2010). Deep versus shallow origin of gravity anomalies, topography and volcanism on Earth, Venus and Mars. *Icarus*, *207*(2), 564–577. https://doi.org/10.1016/j.icarus.2009.12.025
Stein, C., Lowman, J. P., & Hansen, U. (2013). The influence of mantle internal heating on lithospheric mobility: Implications for super-Earths. *Earth and Planetary Science Letters*, *361*, 448–459. https://doi.org/10.1016/j.epsl.2012.11.011
Stofan, E. R., Smrekar, S. E., Mueller, N., & Helbert, J. (2016). Themis Regio, Venus: Evidence for recent (?) volcanism from VIRTIS data. *Icarus*, *271*, 375–386. https://doi.org/10.1016/j.icarus.2016.01.034
Strom, R. G., Schaber, G. G., & Dawson, D. D. (1994). The global resurfacing of Venus. *Journal of Geophysical Research*, *99*(E5) 10899–10926.
Tackley, P. J. (2008). Modelling compressible mantle convection with large viscosity contrasts in a three-dimensional spherical shell using the yin-yang grid. *Physics of the Earth and Planetary Interiors*, *171*(1–4), 7–18. https://doi.org/10.1016/j.pepi.2008.08.005

Tackley, P. J., Ammann, M., Brodholt, J. P., Dobson, D. P., & Valencia, D. (2013). Mantle dynamics in super-Earths: Post-perovskite rheology and self-regulation of viscosity. *Icarus*, *225*(1), 50–61. https://doi.org/10.1016/j.icarus.2013.03.013

Tackley, P. J., & King, S. D. (2003). Testing the tracer ratio method for modeling active compositional fields in mantle convection simulations. *Geochemistry, Geophysics, Geosystems*, *4*(4). https://doi.org/10.1029/2001gc000214

Turcotte, D. L., Morein, G., Roberts, D., & Malamud, B. D. (1999). Catastrophic resurfacing and episodic subduction on Venus. *Icarus*, *139*, 49–54.

Uppalapati, S. (2020). Dynamics of lithospheric overturns and implications for Venus' surface. *Zenodo*. https://doi.org/10.5281/zenodo.3732102

van Heck, H. J. (2011). Scaling of plate tectonics on terrestrial planets, (Doctoral Thesis). https://doi.org/10.3929/ethz-a-6560179.19521

Wei, D., Yang, A., & Huang, J. (2014). The gravity field and crustal thickness of Venus. *Science China Earth Sciences*, *57*(9), 2025–2035. https://doi.org/10.1007/s11430-014-4824-5

Weller, M. B., & Kiefer, W. S. (2020). The physics of changing tectonic regimes: Implications for the temporal evolution of mantle convection and the thermal history of Venus. *Journal of Geophysical Research: Planets*, *125*(1), e2019JE005960https://doi.org/10.1029/2019je005960

Weller, M. B., Lenardic, A., & O'Neill, C. (2015). The effects of internal heating and large scale climate variations on tectonic bi-stability in terrestrial planets. *Earth and Planetary Science Letters*, *420*, 85–94. https://doi.org/10.1016/j.epsl.2015.03.021

Wieczorek, M. A. (2007). The gravity and topography of the terrestrial planets. *Treatise on Geophysics*, *10*, 165–206.

Xie, S., & Tackley, P. J. (2004). Evolution of U-Pb and Sm-Nd systems in numerical models of mantle convection and plate tectonics. *Journal of Geophysical Research*, *109*(B11). https://doi.org/10.1029/2004jb003176